Pergamon

Geochimica et Cosmochimica Acta, Vol. 67, No. 22, pp. 4373–4387, 2003
Copyright © 2003 Elsevier Ltd
Printed in the USA. All rights reserved
0016-7037/03 $30.00 + .00

doi:10.1016/S0016-7037(03)00377-6

Secular evolution of the lithosphere beneath the eastern North China Craton: Evidence from Mesozoic basalts and high-Mg andesites

HONG-FU ZHANG,[1,*] MIN SUN,[2] XIN-HUA ZHOU,[1] MEI-FU ZHOU,[2] WEI-MING FAN,[1] and JIAN-PING ZHENG[3]

[1]Laboratory of Lithosphere Tectonic Evolution, Institute of Geology and Geophysics, Chinese Academy of Sciences, P.O. Box 9825, Beijing 100029, P.R. China

[2]Department of Earth Sciences, The University of Hong Kong, Pokfulam Road, Hong Kong, P.R. China

[3]Faculty of Earth Sciences, China University of Geosciences, Wuhan 430074, P.R. China

(*Received December* 2, 2002; *accepted in revised form May* 12, 2003)

Abstract—Geochemical and isotopic data from Mesozoic lavas from the Jianguo, Niutoushan, Wulahada, and Guancaishan volcanic fields on the northern margin of the North China Craton provide evidence for secular lithospheric evolution of the region. Jianguo lavas are alkaline basalts with LILE- and LREE-enrichment ($(La/Yb)_N$=12.2–13.2) and MORB-like Sr-Nd-Pb isotopic ratios ($(^{87}Sr/^{86}Sr)_i$<0.704; ε_{Nd}=3.9–4.8; $(^{206}Pb/^{204}Pb)_i \approx 18$). Niutoushan basalts are similar but show evidence of olivine fractionation. Wulahada lavas are high-Mg andesites (Mg#~67) with EM1 Sr-Nd-Pb isotopic signatures. Geochemical data suggest that the basalts originated from MORB-type asthenosphere whereas the high-Mg andesites were derived an EM1 mantle source, i.e., a refractory lithospheric mantle modified by a previously subducted slab. The result, combined with the available data of the Mesozoic basalts from the southern portion of the NCC (Zhang et al., 2002), manifests a vast secular evolution of the lithospheric mantle beneath the eastern NCC from the Paleozoic refractory continental lithosphere to this Mesozoic modified lithosphere. Compared with the cratonic margin, the lithospheric mantle beneath the center of the craton was less extensively modified, implying the secular evolution was related to the subduction processes surrounding the NCC. Therefore, we suggest that the interaction of the slab-derived silicic melt with the old refractory lithospheric mantle converted the Paleozoic cratonic lithospheric mantle into the late Mesozoic fertile mantle, which was also different from the Cenozoic counterpart. A geodynamic model is proposed to illustrate such a secular lithosphere evolution. *Copyright © 2003 Elsevier Ltd*

1. INTRODUCTION

The lithospheric mantle of the North China Craton (NCC) has attracted considerable attention over the last two decades, due to a dramatic change from a Paleozoic cratonic mantle to a Cenozoic "oceanic" lithospheric mantle (Griffin et al., 1992, 1998; Menzies et al., 1993; Menzies and Xu, 1998; Fan et al., 2000; Xu, 2001; O'Reilly et al., 2001). This change requires considerable thinning of the lithosphere during the Phanerozoic, which may have occurred in the Mesozoic. The cause of this change is hotly debated. Menzies et al. (1993) suggested that destabilization of the cratonic lithosphere was initiated by the Indo-Eurasian collision, whereas Zheng (1999), Zheng et al. (2001) and Poudjom Djomani et al. (2001) proposed that the Archean cratonic lithosphere was replaced by young Phanerozoic lithosphere resulting in removal of the Archean lithospheric keel. The presence of both high- and low- magnesian olivines in spinel-facies peridotitic xenoliths entrained in the Cenozoic basalts from the Hebi area, Henan Province (Zheng et al., 2001) support such a replacement model. Gao et al. (2002) proposed that the lithospheric replacement beneath the Hannuoba region might have occurred as early as the Proterozoic (1.9 Ga), based on Re-Os isotopic data for mantle xenoliths from Hannuoba basalts. Menzies and Xu (1998) and Xu (2001) emphasized the importance of thermo-mechanical erosion from the base of the lithosphere and subsequent chemical erosion resulting from asthenosphere upwelling. Based on the formation of Mesozoic basins, Menzies and Xu (1998) argued that thermal and chemical erosion of the lithosphere in the Jurassic was triggered by circum-craton subduction and subsequent passive continental extension. However, these suggestions did not consider detailed replacement processes.

Geochemical data on the Mesozoic basalts from Fangcheng (Fig. 1a) in the Southern part of the NCC (SNCC) suggest enrichment of the source region by silicic melts (Zhang et al., 2002; Zhang and Sun, 2002), perhaps produced by subduction of Yangtze crust underneath the old lithosphere during the Jurassic. Thus, subduction of Yangtze crust and subsequent collision between the two cratons could have played an important role in the evolution of the SNCC lithosphere (Zhang et al., 2002). This interpretation is based on data from Mesozoic mantle-derived basalts and alkaline intrusive complexes in the SNCC (Fan et al., 2001; Zhang et al., 2002; Zhang and Sun, 2002).

Mesozoic basaltic-andesitic volcanic rocks are also widespread in northern NCC (NNCC, Chen et al., 1997; 1999). These Jurassic-Cretaceous lavas provide an excellent opportunity to probe the underlying lithospheric mantle. We selected a suite of newly-discovered, xenolith-bearing basalts and basaltic andesites from the region (Fig. 1b) for detailed analysis. The new geochemical data provide important constraints on the petrogenesis of the Mesozoic basalts and basaltic andesites and on their mantle sources beneath the NNCC. Using these data, together with previously published data from the SNCC, we attempt to identify spatial and

* Author to whom correspondence should be addressed (hfzhang@mail.igcas.ac.cn).

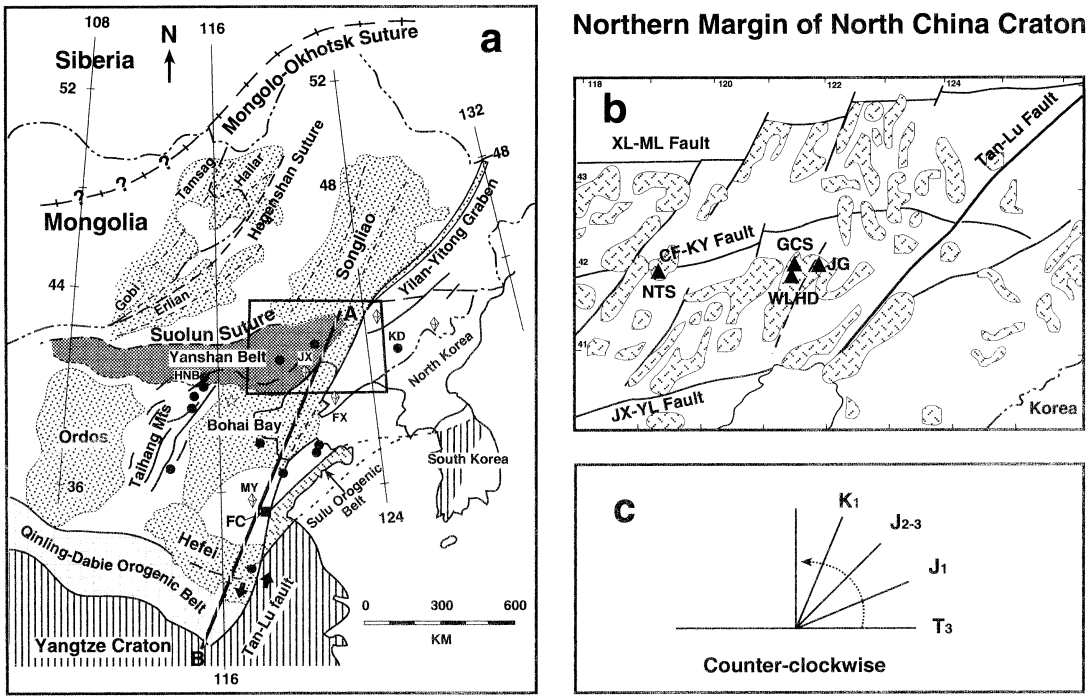

Fig. 1. (a) Simplified geological map showing the major tectonic units of the North China Craton and its surrounding areas: the Mesozoic sedimentary basins (stippled fields) and the localities of Paleozoic kimberlites (open diamond), Mesozoic Fangcheng basalts (filled square), and Cenozoic basalts (filled circle) on the NCC (modified from Davis et al., 2001 and Fan et al., 2000). Dashed lines within the Mesozoic sedimentary basins are the trends of Jurassic-Cretaceous extensional faults. Between the Suolun Suture and the Mongolo-Okhotsk Suture is the Central Asian Orogenic Belt (Şengör et al.; 1999). The Hegenshan suture is schematically shown from Robinson et al. (1999). Line A-B shows the direction of the cross section in Fig. 6. FC, MY, FX, JX, KD, and HNB represent Fangcheng, Mengyin, Fuxian, Jingxi, Kuandian, and Hannuoba. (b) Schematic illustration for the distribution of Mesozoic volcanic rocks on the NNCC and sampling locations (modified from Chen et al., 1997). Xilamulun (XL-ML) River Fault is an important fault zone, which together with the Suolun suture marks the northern boundary of the NCC. Chifeng-Kaiyuan (CF-KY) Fault and Jingxi-Yaolu (JX-YL) Fault are two NEE-SWW-trending faults, dividing the northeastern NCC into three regions. JG, GCS, WLHD, and NTS represent the Jianguo, Guancaishan, Wulahada, and Niutoushan volcanic fields, respectively. (c) Schematically shown are the orientations of the long axes of major Mesozoic sedimentary basins developed in Liaoxi region. Note that the Mesozoic tectonic lineation and orientation of sedimentary basins changed with time, in a counter-clockwise direction from EW in the late Triassic, to NEE-NE in the J_1 and J_{2-3}, to NNE in the early Cretaceous.

temporal variations in the Mesozoic lithospheric mantle across the eastern NCC.

2. REGIONAL GEOLOGY

The North China Craton is bounded on the south by the Paleozoic to Triassic Qinling-Dabie-Sulu orogenic belt (Li et al., 1993; Meng and Zhang, 2000) and on the north by the Central Asian Orogenic Belt (Fig. 1a; Şengör et al., 1999; Davis et al., 2001).

The Qinling-Dabie-Sulu belt was resulted from the continental collision between the NCC and the Yangtze Craton in the Triassic (Li et al., 1993). The belt comprises of eclogites and a variety of gneisses, which were derived from the Yangtze Craton (Xu et al., 1992; Liu et al., 2001). The finding of diamond and coesite in the eclogites (Xu et al., 1992) and coesite inclusions in zircons from both ortho- and para-gneisses (Liu et al., 2001) demonstrate that the upper and middle crustal units of the Yangtze Craton were subducted to ultrahigh pressure conditions (Liu et al., 2001). The exsolution lamellae of clinopyroxene, rutile and apatite in garnets from the eclogite suggest that the subduction of the Yangtze crust reached to depths greater than 200 km (Ye et al., 2000). This subduction and the subsequent collision may have significantly affected the lithospheric mantle beneath the SNCC.

To the north of the NCC, the generally EW-trending Central Asian Orogenic Belt was formed through south-directed subduction and arc-arc, arc-continent, and continent-continent collision mainly during the Paleozoic (Robinson et al., 1999; Davis et al., 2001; Buchan et al., 2002). During this time multiple Ordovician to Permian oceanic arcs and the Mongolian microcontinent were amalgamated to the active margin of the NCC (Davis et al., 2001). The widespread occurrence of Paleozoic ophiolites, Paleozoic to Triassic blueschists, and synchronous igneous rocks suggests that the southward subduction commenced in the early Paleozoic and that the final collision occurred in the Triassic (Xu and Chen, 1997; Robinson et al., 1999; Davis et al., 2001; Buchan et al., 2002). The Suolun suture and the Xilamulun Fault mark the southern boundary of this belt (Fig. 1a and b). The uplift of the Yanshan belt and the extensive Yanshanian magmatism in the NNCC

Table 1. K-Ar ages on whole rock powders. Parameters for ^{40}K: $\lambda_e = 0.581 \times 10^{-10}$ year^{-1}; $\lambda_\beta = 4.962 \times 10^{-10}$ year^{-1}; $^{40}K = 0.01167$ atom% (Steiger and Jäger, 1977). TA: Trachy-andesite. a: Lower sequence; b: Upper sequence.

Locality	Sample	Rock	Weight (g)	K (%)	^{40}Ar total 10^{-10} (mol/g)	^{40}Ar radiogenic 10^{-10} (mol/g)	^{40}K 10^{-8} (mol/g)	Age ($\pm 2\sigma$) (Ma)
Jianguo	JG-01	Basalt	0.01546	1.55	3.754	2.774	4.626	100.4 ± 1.6
Wulahada	WLHD-01	High-Mg andesite	0.01604	1.39	6.880	3.570	4.149	142.4 ± 2.2
Guancaishan	GCS-02	Andesite	0.01564	2.06	6.818	4.994	6.148	134.6 ± 2.0
Niutoushan	NTS-01	Basaltic TA[a]	0.01557	2.54	6.635	4.870	7.581	107.3 ± 1.6
Niutoushan	NTS-07	Phono-Tephrite[b]	0.01579	2.86	6.227	4.794	8.536	94.2 ± 1.4

may be a consequence of this southward subduction and the subsequent collision (Fig. 1a) (Davis et al., 2001).

The NCC is composed of two Archean continental nuclei, the Eastern Block and the Western Block, separated by a Proterozoic orogenic belt geographically corresponding to the Taihang Mountains (Zhao et al., 2002 and references therein). The craton has a basement of dominantly Archean to Paleoproterozoic TTG (tonalitic-trondhjemitic-granodioritic) gneisses and metavolcanic and metasedimentary rocks, covered by Sinian-Ordovician marine sedimentary rocks, Carboniferous-Permian continental clastic rocks, and Mesozoic basin deposits (Zhao et al., 2002). In the Western Block, the cratonic lithosphere has been stable since Precambrain. However, extensive volcanism in the Eastern Block is indicated by Paleozoic kimberlites, Mesozoic volcanic and plutonic rocks, and Cenozoic basalts (Fig. 1a). Voluminous Jurassic-Cretaceous volcanic rocks were erupted into a series of small Mesozoic fault- and rift-related or subsidence basins in the NNCC (Fig. 1b) (Chen et al., 1997, 1999; Davis et al., 2001; Ren et al., 2002). These basins were aligned in an EW direction in the late Triassic, but shifted to a dominantly NNE direction in the early Cretaceous (Fig. 1c).

In the study area, four major periods of volcanism have been identified (Chen et al., 1997): early Jurassic (Xinglonggou Formation), mid-Jurassic (Lanqi Formation), early Cretaceous (Yixian Formation), and late early Cretaceous (Fuxin Formation). Volcanic rocks of the Xinglonggou Formation were limited and occur along Tan-Lu fault (Chen et al., 1997). The Lanqi Formation is more extensive and records several cycles of eruption, each beginning with high-Mg andesites and ending with trachyites and tuffs. The Yixian Formation is most voluminous, which is 1000–2000 m thick and consists dominantly of andesites, trachyandesites, and trachyites. The Fuxin Formation consists of scattered central-type volcanoes composed of basalt. These lavas were erupted about 100 Ma ago, extensively eroded and primarily preserved as volcanic conduits, such as those at Jianguo and Niutoushan (Fig. 1b).

3. PETROGRAPHY

Fresh lavas were sampled from the Jianguo, Wulahada and Guancaishan volcanic fields of the Fuxin-Yixian basin, Liaoning Province, and from the Niutoushan volcanic field of the Pingzhuang basin, Inner Mongolia (Fig. 1b). The Jianguo basalts (Table 1 and Fig. 1b) are dark gray in colour, massive, and with well-developed columnar joints. Most rocks possess sparse olivine and plagioclase phenocrysts and contain small (dominantly 1–4 cm) spinel-facies mantle xenoliths. Xenoliths of amphibole-bearing spinel lherzolite, plagioclase-bearing pyroxenite and lower crustal rocks have also been reported in late Cretaceous trachybasalts of the region (Xu et al., 1999). The Niutoushan lavas, which eruped about 107–94 Ma ago (Table 1), occur near Pingzhuang village of Chifeng city, south of the Chifeng-Kaiyuan fault (Fig. 1b). These lavas are similar to the Jianguo basalts but are generally lack olivine phenocrysts. Pieces of mantle xenoliths are also present in the Niutoushan lavas, but they are too small to be analyzed (less than 1 cm). The Wulahada and Guancaishan lavas occur in the Fuxin-Yixian basin, close to the Jianguo basalts, and were erupted 142 and 134 Ma ago, respectively (Table 1). The Wulahada lavas are dark gray and massive but lack columnar jointing. All of these rocks are porphyritic with euhedral olivine phenocrysts. The Guancaishan lavas are light gray and relatively coarse-grained with well-developed columnar joints. These rocks commonly contain abundant phenocrysts of plagioclase and pyroxene (2 to 6 mm).

4. ANALYTICAL METHODS

Fresh rock samples free of xenocrysts were selected and ground with an agate mill. Whole-rock K-Ar age determinations were carried out on a MM5400 mass spectrometer at the Research Institute of Petroleum Exploration and Development, China National Petroleum Cooperation. Major oxides and trace elements were analyzed with ICP-AES at Guangzhou Institute of Geochemistry and ICP-MS at Guiyang Institute of Geochemistry, Chinese Academy of Geosciences (CAS), respectively. Samples were digested with $HF+HNO_3$ for major element analysis, following the procedures of Li et al. (2002). The analytical precisions for major oxides were better than 5%, estimated from repeat analyses of the standards (BHVO-1, G-2, GSR-1). For trace element analyses, whole rock powders were weighed and then dissolved in distilled $HF+HNO_3$ in 15 mL Savillex Teflon screw-cap beakers at 100°C for 2 d, while those andesitic samples were dissolved in screw top PTFE-lined stainless bombs at 190°C, dried, digested with 6M HCl at 150°C for 4 d, and then diluted to 100 mL before analysis. A blank solution was prepared and the total procedural blanks were <50 ng for all the trace elements reported in this paper. Analytical calibration was accomplished with the aqueous standard solutions. Rhodium was used as an internal standard to correct matrix effects and instrument drift. Five standard reference materials (GSR-1, GBPG-1, BHVO-1, NIM-G, and OU-6) were also used to check the accuracy and precision and the results were in agreement with the recommended values. Detailed sample preparation and analytical method are given in Qi et al. (2000).

For Sr-Nd isotope analyses, sample powders were spiked with mixed isotope tracers, dissolved in Teflon capsules with $HF+HNO_3$ acid, and separated by conventional cation-exchange techniques. The isotopic measurements were performed on a VG-354 mass-spectrometer at the Institute of Geology and Geophysics (IGG), CAS. The mass fractionation corrections for Sr and Nd isotopic ratios were based on $^{86}Sr/^{88}Sr = 0.1194$ and $^{146}Nd/^{144}Nd = 0.7219$. Repeat analyses yielded a $^{87}Sr/^{86}Sr$ ratio of 0.71023 ± 0.00006 for the NBS-987 Sr standard and a $^{143}Nd/^{144}Nd$ ratio of 0.511845 ± 0.000012 for the La Jolla standard. For Pb isotope determinations, 200 mg of powder were weighed into a Teflon vial, spiked and dissolved in concentrated HF at 80°C for 72 h.

Table 2. Major oxides (wt%) in the Mesozoic volcanic lavas from the northern margin of the NCC. LOI = Loss on Ignition; Mg# = Mg/(Mg+TFeO) atomic ratio.

	Jianguo									Wulahada					
	JG-01	JG-02	JG-03	JG-04	JG-05	JG-06	JG-07	JG-08	JG-09	WLHD-01	WLHD-02	WLHD-03	WLHD-04	WLHD-05	WLHD-06
SiO_2	44.84	45.48	44.82	45.92	45.01	46.07	43.40	45.50	44.82	52.96	52.47	55.00	53.70	55.32	57.07
TiO_2	2.92	2.89	2.93	2.85	2.95	2.88	2.95	2.85	2.93	1.11	1.08	1.05	1.09	1.06	1.01
Al_2O_3	14.79	14.51	14.81	14.27	14.59	14.36	14.88	14.37	14.81	14.80	14.80	14.35	14.63	14.24	13.40
Fe_2O_3	11.57	11.51	11.68	11.37	11.78	11.38	11.78	11.51	11.75	8.02	7.91	7.67	7.95	7.77	7.39
MnO	0.17	0.17	0.17	0.17	0.17	0.17	0.17	0.17	0.17	0.11	0.12	0.11	0.11	0.11	0.11
MgO	8.31	8.25	8.38	8.09	8.30	8.06	8.39	8.16	8.30	8.06	8.27	8.05	8.28	7.91	7.52
CaO	10.27	10.34	10.52	10.11	10.32	10.07	10.32	10.27	10.62	7.28	7.01	6.65	6.90	6.88	6.62
Na_2O	3.19	2.70	3.00	3.03	3.33	3.18	3.33	3.09	3.03	3.68	3.71	3.55	3.65	3.52	3.39
K_2O	1.88	1.93	1.93	1.80	1.91	1.80	1.91	1.87	1.78	1.84	1.89	1.82	1.87	1.76	1.69
P_2O_5	0.64	0.62	0.65	0.62	0.66	0.63	0.66	0.63	0.63	0.31	0.30	0.29	0.32	0.30	0.28
LOI	1.33	1.55	1.25	1.57	1.38	1.47	1.34	1.52	1.17	1.53	1.66	1.56	1.50	1.63	1.85
	99.9	100.0	100.1	99.8	100.4	100.1	99.1	99.9	100.0	99.7	99.2	100.1	100.0	100.5	100.3
Mg#	58.7	58.7	58.7	58.5	58.2	58.4	58.5	58.4	58.3	66.6	67.4	67.5	67.3	66.8	66.8

	Niutoushan									Guancaishan					
	NTS-01	NTS-02	NTS-03	NTS-04	NTS-05	NTS-06	NTS-07	NTS-08	NTS-09	GCS-01	GCS-02	GCS-03	GCS-04	GCS-05	GCS-06
SiO_2	50.40	48.87	49.26	48.81	48.53	48.66	47.98	51.30	55.51	61.84	60.31	60.37	61.80	60.82	63.53
TiO_2	1.71	1.86	1.79	1.79	1.82	1.85	1.87	1.74	1.10	0.74	0.77	0.77	0.74	0.77	0.70
Al_2O_3	16.83	18.21	17.49	17.40	18.01	18.22	18.43	17.04	15.51	16.22	16.89	16.77	16.32	17.14	15.49
Fe_2O_3	6.96	7.58	7.34	7.24	7.48	7.48	7.55	7.15	7.45	5.57	5.99	5.91	5.57	5.97	5.10
MnO	0.12	0.13	0.12	0.12	0.12	0.13	0.13	0.12	0.10	0.09	0.09	0.09	0.09	0.10	0.08
MgO	5.60	5.34	5.62	5.87	5.79	5.85	5.49	5.20	4.24	2.64	2.83	2.71	2.57	2.73	2.44
CaO	6.05	6.43	6.44	6.29	6.44	6.52	6.27	5.98	5.93	4.83	5.09	5.04	4.90	5.14	4.54
Na_2O	4.41	5.34	4.66	4.67	4.75	4.82	5.90	5.41	3.98	3.75	3.92	3.80	3.72	3.90	3.50
K_2O	2.97	3.47	3.09	3.10	3.25	3.26	3.47	2.98	2.57	2.52	2.63	2.53	2.48	2.64	2.39
P_2O_5	0.82	0.88	0.85	0.85	0.86	0.87	0.89	0.82	0.57	0.22	0.23	0.22	0.22	0.23	0.21
LOI	3.37	2.67	3.46	3.25	3.18	3.09	2.64	2.79	2.41	1.77	1.81	1.30	1.50	0.91	1.44
	99.2	100.8	100.1	99.4	100.2	100.8	100.6	100.5	99.4	100.2	100.6	99.5	99.9	100.4	99.4
Mg#	61.4	58.2	60.3	61.6	60.5	60.8	59.0	59.0	53.0	48.4	48.3	47.6	47.7	47.5	48.6

Pb was separated and purified by conventional cation-exchange techniques (AG1×8, 200–400 resin) with diluted HBr as an eluant. Isotopic ratios were measured with the VG-354 mass-spectrometer at IGG. Repeat analyses of NBS981 yielded $^{204}Pb/^{206}Pb = 0.05897\pm15$, $^{207}Pb/^{206}Pb = 0.91445\pm80$, $^{208}Pb/^{206}Pb = 2.16170\pm180$. Detailed descriptions of the analytical techniques are given elsewhere (Zhang et al., 2002 and references therein). All analytical results are presented in Tables 1, 2, 3, 4.

5. RESULTS

Jianguo basalts: The Jianguo lavas are alkaline basalts with uniform major oxide, trace element and Sr-Nd-Pb isotopic compositions (Figs. 2, 3, 4, 5). These rocks have low silica (SiO_2=43.4–45.9%) and high alkalis (Na_2O+K_2O=4.6–5.2%), and lie in the fields of basalt-trachybasalt-tephrite in the SiO_2 vs. Na_2O+K_2O diagram (Le Maitre et al., 1989). These rocks have high contents of MgO, FeO^T, CaO, TiO_2, MnO, and transition metal elements (Sc, Cr, Ni) and low in Pb (Fig. 2), with moderate enrichment of LREE (ΣREE=180–196 ppm, $(La/Yb)_N$=12.2–13.2) and LILE (Cs, Ba, Rb, Sr, U, and Th), without depletion of HFSE (Nb, Ta, Zr, Hf, and Ti) (Fig. 3a&b). All samples from the Jianguo basalts have low Sr, and high Nd and Pb isotopic ratios [$(^{87}Sr/^{86}Sr)_i<0.704$; ε_{Nd}=3.9–4.8, $(^{206}Pb/^{204}Pb)_i \approx 18$] (Table 4 and Figs. 4 and 5). Low $^{207}Pb/^{204}Pb$ ($\Delta7/4 = -8\sim0.9$) and high $^{208}Pb/^{204}Pb$ ($\Delta8/4$=8.3–41.2) ratios are also apparent in these basalts. These samples are significantly different from the Mesozoic Fangcheng basalts on the SNCC (Figs. 2–5), but have similar Sr-Nd isotopes to Cenozoic basalts from the NCC (such as Hannuoba and Kuandian) and oceanic basalts (i.e., MORBs and OIBs).

Niutoushan basalts: The Niutoushan lavas are dominantly phono-tephrites with low MgO (<6%), FeO^T, and CaO (5.9~6.5%) and high SiO_2 (48~55.5%), Al_2O_3 (>16%), P_2O_5 (>2.4%) and alkalis (Na_2O+K_2O>7%) (Fig. 2). A few trachyandesites are present in the upper part of the sequence. These rocks are enriched in LREE (ΣREE=211–227 ppm, $(La/Yb)_N$=17.5–20.2) and LILE, without depletion of HFSE (Table 3 and Fig. 3c&d). The Niutoushan basalts have rather unradiogenic Sr-Nd-Pb isotopic compositions [$(^{87}Sr/^{86}Sr)_i<0.7042$), ε_{Nd} (>1.5) and high ($^{206}Pb/^{204}Pb)_i$] (Table 4), similar to the values for the Tertiary Hannuoba and Quaternary Kuandian basalts (Figs. 4 and 5).

Wulahada high-Mg basaltic andesites: The Wulahada lavas are characterized by high MgO (Mg#~67) and SiO_2 (>52.5%) and low Al_2O_3, TiO_2, and alkalis (Table 2 and Fig. 2). These rocks are classified as high-Mg basaltic andesites according to Crawford et al. (1989). The samples have low concentrations of most trace elements except for Cs and Pb (ΣREE<128 ppm) (Table 3), despite showing enrichment of LILE and LREE $(La/Yb)_N$=11.5–12.6) (Fig. 3e&f). They

Table 3. Trace element concentrations (ppm) in the Mesozoic volcanic lavas from the northern margin of the NCC.

	Jianguo									Wulahada					
	JG-01	JG-02	JG-03	JG-04	JG-05	JG-06	JG-07	JG-08	JG-09	WLHD-01	WLHD-02	WLHD-03	WLHD-04	WLHD-05	WLHD-06
La	37.1	37.8	38.8	38.9	40.4	38.4	38.9	39.2	39.9	25.83	25.74	26.06	25.75	25.92	25.45
Ce	73.3	75.7	78.2	77.7	79.7	77.3	76.4	78.3	79.8	53.04	52.26	53.34	51.88	54.08	53.37
Pr	8.10	8.38	8.76	8.52	8.88	8.61	8.65	8.74	8.99	6.47	5.92	5.87	5.80	5.95	5.75
Nd	34.1	34.9	36.0	36.5	36.8	34.9	35.8	36.5	36.8	23.26	23.22	23.29	23.08	23.73	22.71
Sm	7.18	7.46	7.73	7.55	7.68	7.30	7.15	7.84	7.70	4.60	4.27	4.79	4.36	4.30	4.46
Eu	2.20	2.27	2.30	2.33	2.31	2.33	2.31	2.33	2.38	1.33	1.31	1.39	1.27	1.38	1.36
Gd	6.35	6.74	6.76	6.90	6.77	6.58	6.84	6.47	6.83	3.89	4.04	3.97	3.75	4.01	3.76
Tb	0.94	0.94	0.98	0.95	1.04	0.93	0.94	0.95	0.99	0.60	0.54	0.55	0.54	0.60	0.57
Dy	5.12	5.09	5.18	5.34	5.43	5.41	5.21	5.37	5.72	3.17	3.20	3.30	3.12	3.41	3.39
Ho	0.92	0.93	0.93	1.00	1.00	0.98	0.99	0.99	0.97	0.59	0.61	0.61	0.58	0.62	0.64
Er	2.50	2.55	2.60	2.80	2.66	2.67	2.63	2.60	2.86	1.74	1.75	1.83	1.76	1.73	1.81
Tm	0.30	0.34	0.34	0.35	0.34	0.34	0.34	0.33	0.32	0.24	0.22	0.25	0.22	0.25	0.24
Yb	2.04	2.01	2.16	2.17	2.16	2.01	2.20	2.23	2.10	1.42	1.45	1.48	1.55	1.53	1.52
Lu	0.28	0.27	0.29	0.29	0.32	0.28	0.27	0.30	0.30	0.22	0.19	0.23	0.19	0.22	0.23
Y	25.8	26.0	26.5	25.6	27.3	25.8	26.3	26.0	27.2	17.03	16.73	17.39	16.97	19.81	16.92
Cs	0.41	0.44	0.46	0.44	0.44	0.46	0.39	0.44	0.46	2.28	2.11	2.38	2.19	2.23	2.36
Ba	736	756	771	765	774	859	742	770	786	696.3	701.9	736.2	663.0	725.2	737.2
Rb	46.8	52.2	52.3	49.1	51.1	47.7	48.6	52.9	52.3	45.44	45.23	45.72	44.89	46.40	46.78
Sr	628	964	742	758	726	716	747	749	581	695.6	728.0	810.9	770.0	744.4	796.3
Nb	60.7	62.1	64.5	63.4	65.6	61.9	62.7	65.6	64.3	11.39	11.29	11.34	11.29	11.56	11.03
Ta	3.49	3.56	3.54	3.65	3.83	3.61	3.51	3.69	3.73	0.63	0.63	0.65	0.64	0.68	0.65
Zr	198	205	208	206	213	204	203	212	212	142.4	140.6	139.5	139.1	142.4	141.1
Hf	4.9	5.24	5.27	5.45	5.48	5.22	5.15	5.20	5.37	3.58	3.62	3.66	3.49	3.61	3.59
U	1.12	1.17	1.16	1.21	1.19	1.24	1.17	1.19	1.21	0.98	0.94	0.96	0.94	0.96	0.96
Th	4.47	4.58	4.72	4.8	4.99	4.86	4.73	4.92	4.87	4.11	4.00	4.15	3.98	4.22	4.02
Pb	3.36	3.1	3.09	4.03	4.89	3.84	3.97	3.27	3.39	6.44	9.96	6.48	6.25	8.54	6.14
Cr	616	619	626	709	633	597	611	670	668	784.2	763.7	788.9	750.7	851.8	818.2
Ni	162	166	172	197	166	156	169	174	178	179.8	183.2	194.9	181.6	211.7	182.4
ΣREE	180.4	185.4	191	191.3	195.5	188	188.6	192.2	195.7	126.4	124.7	127.0	123.8	127.7	125.2
$(La/Yb)_N$	12.6	13.0	12.4	12.4	12.9	13.2	12.2	12.2	13.2	12.6	12.3	12.2	11.5	11.8	11.6

	Guancaishan						Niutoushan								
	GCS-01	GCS-02	GCS-03	GCS-04	GCS-05	GCS-06	NTS-01	NTS-02	NTS-03	NTS-04	NTS-05	NTS-06	NTS-07	NTS-08	NTS-09
La	30.14	29.73	30.25	30.22	29.35	30.90	55.06	56.88	54.46	54.59	53.49	54.99	53.71	51.65	57.57
Ce	60.93	59.28	60.82	60.45	58.67	62.01	93.56	99.05	94.80	93.99	94.98	94.81	94.18	92.71	98.09
Pr	6.70	6.44	6.58	6.50	6.51	6.74	9.54	9.77	9.62	9.29	9.56	9.68	9.43	9.11	9.71
Nd	24.91	25.29	25.52	25.59	24.38	25.52	34.02	36.46	34.63	34.62	34.86	35.13	34.57	34.24	36.31
Sm	4.59	4.66	4.90	4.60	4.38	4.86	5.83	6.53	6.38	6.16	5.78	6.10	5.82	6.16	6.38
Eu	1.14	1.21	1.18	1.10	1.11	1.20	1.82	1.99	1.91	1.91	1.95	1.88	1.95	1.88	1.92
Gd	3.94	3.95	4.21	4.00	4.04	4.12	5.26	5.41	5.38	5.13	5.38	5.13	5.33	5.18	5.22
Tb	0.61	0.58	0.60	0.61	0.56	0.60	0.71	0.78	0.71	0.74	0.74	0.75	0.76	0.71	0.79
Dy	3.40	3.35	3.41	3.36	3.30	3.35	4.15	4.56	4.06	4.09	4.21	4.07	4.07	4.23	4.30
Ho	0.64	0.62	0.65	0.62	0.62	0.66	0.76	0.80	0.82	0.80	0.76	0.78	0.81	0.75	0.79
Er	1.96	1.76	1.99	1.93	1.85	1.92	2.19	2.37	2.29	2.19	2.24	2.27	2.24	2.27	2.27
Tm	0.28	0.27	0.26	0.25	0.25	0.27	0.32	0.31	0.31	0.32	0.33	0.33	0.32	0.29	0.31
Yb	1.79	1.73	1.77	1.81	1.59	1.76	1.92	2.12	2.13	1.93	2.06	2.18	2.08	2.00	1.98
Lu	0.22	0.24	0.25	0.25	0.22	0.24	0.31	0.29	0.29	0.28	0.28	0.31	0.30	0.28	0.31
Y	19.02	18.95	20.02	19.27	19.29	19.85	21.65	23.11	22.35	21.21	22.19	21.97	21.71	22.29	23.02
Cs	2.70	2.61	2.58	2.65	2.52	2.70	1.77	1.86	2.05	1.83	1.89	1.73	1.54	1.59	1.58
Ba	798.1	740.0	772.4	804.7	732.5	806.1	1244.5	1273.3	1258.0	1333.1	1245.8	1253.0	1290.0	1274.5	1296.5
Rb	93.14	90.68	93.28	93.40	88.78	97.76	98.23	101.70	99.43	86.92	85.94	92.43	91.59	79.67	96.50
Sr	606.4	596.3	636.2	633.8	616.6	630.0	1044.1	1070.9	1074.7	1009.6	1087.2	1115.6	963.7	1018.0	1040.2
Nb	11.33	11.30	11.38	11.42	11.29	11.60	95.05	98.75	96.85	97.74	97.60	97.25	98.05	96.16	100.99
Ta	0.83	0.79	0.80	0.79	0.75	0.81	5.41	5.68	5.41	5.43	5.45	5.47	5.41	5.34	5.64
Zr	179.1	176.3	179.7	176.7	176.0	182.6	266.3	279.4	274.4	266.5	277.5	273.4	275.1	273.2	279.4
Hf	4.76	4.65	4.68	4.54	4.53	4.88	5.83	6.22	6.01	5.88	6.16	6.00	6.26	5.94	6.13
U	2.65	2.50	2.45	2.39	2.40	2.59	2.39	2.63	2.42	2.42	2.47	2.46	2.52	2.41	2.55
Th	8.86	8.62	8.74	8.62	8.53	8.88	10.18	10.67	10.06	10.01	10.16	10.31	10.26	10.00	10.71
Pb	13.79	11.73	12.30	13.81	11.71	13.04	5.68	6.47	5.65	5.38	6.12	5.71	6.48	5.25	6.09
Cr	382.0	367.5	392.1	390.6	391.5	418.9	436.5	421.0	426.6	397.0	413.1	443.5	434.6	426.7	430.3
Ni	18.9	15.8	14.8	15.0	14.7	18.2	61.3	59.7	62.0	60.0	60.8	67.9	65.1	59.4	66.3
ΣREE	141.2	139.1	142.4	141.3	136.8	144.1	215.4	227.3	217.8	216.0	216.6	218.4	215.6	211.4	225.9
$(La/Yb)_N$	11.7	11.9	11.9	11.6	12.8	12.2	19.9	18.5	17.7	19.6	18.0	17.5	17.9	17.9	20.2

Table 4. Sr-Nd-Pb isotopes of the Mesozoic volcanic lavas. Chondrite Uniform Reservoir (CHUR) values ($^{87}Rb/^{86}Sr = 0.0847$, $^{87}Sr/^{86}Sr = 0.7045$, $^{147}Sm/^{144}Nd = 0.1967$, $^{143}Nd/^{144}ND = 0.512638$) are used for the calculation. $\lambda_{Rb} = 1.42 \times 10^{-11}$ year^{-1}, $\lambda_{Sm} = 6.54 \times 10^{-12}$ year^{-1}, $\lambda_{U238} = 1.55125 \times 10^{-10}$ year^{-1}, $\lambda_{U235} = 9.8485 \times 10^{-10}$ year^{-1}, $\lambda_{Th232} = 4.9475 \times 10^{-11}$ year^{-1} (Steiger & Jäger, 1977 and Lugmair & Marti, 1978). Initial isotope ratios were obtained by assuming eruption age in Table 1. $\Delta 7/4 = [(^{207}Pb/^{204}Pb)_i - (^{207}Pb/^{204}Pb)_{NHRL}] \times 100$; $\Delta 8/4 = [(^{208}Pb/^{204}Pb)_i - (^{208}Pb/^{204}Pb)_{NHRL}] \times 100$; $(^{207}Pb/^{204}Pb)_{NHRL} = 0.1084 \times (^{206}Pb/^{204}Pb)_i + 13.491$ (Hart, 1984); $(^{208}Pb/^{204}Pb)_{NHRL} = 1.209 \times (^{206}Pb/^{204}Pb)_i + 15.627$ (Hart, 1984).

	$^{87}Rb/^{86}Sr$	$^{87}Sr/^{86}Sr$	$^{87}Sr/^{86}Sr_1$	$^{147}Sm/^{144}Nd$	$^{143}Nd/^{144}Nd$	$^{143}Nd/^{144}Nd_1$	ε_{ND}	$^{206}Pb/^{204}Pb$	$^{207}Pb/^{204}Pb$	$^{208}Pb/^{204}Pb$	$^{208}U/^{204}Pb$	$^{206}Pb/^{204}Pb_1$	$^{207}Pb/^{204}Pb_1$	$^{208}Pb/^{204}Pb_1$	$\Delta 7/4$	$\Delta 8/4$
JG-01	0.2154	.703730	.703423	0.1273	.512840	.512756	4.83	18.322	15.398	37.894	20.93	17.994	15.383	37.464	−5.9	8.3
JG-02	0.1565	.704300	.704077	0.1292	.512795	.512710	3.93	18.240	15.436	38.083	23.74	17.867	15.419	37.605	−0.9	37.7
JG-03	0.2038	.703605	.703314	0.1298	.512804	.512719	4.10	18.251	15.456	38.025	23.66	17.880	15.438	37.530	0.9	28.6
JG-04	0.1873	.703930	.703663	0.1250	.512814	.512732	4.35	18.302	15.457	38.147	18.92	18.005	15.443	37.760	0.0	36.5
JG-05	0.2035	.703810	.703520	0.1262	.512823	.512740	4.51	18.320	15.457	38.233	15.36	18.079	15.446	37.901	−0.5	41.7
JG-06	0.1926	.703736	.703461	0.1264	.512808	.512725	4.22	18.264	15.371	37.942	20.26	17.946	15.356	37.533	−8.0	21.0
JG-07	0.1881	.703969	.703701	0.1207	.512812	.512733	4.37	18.297	15.451	38.191	18.58	18.005	15.437	37.804	−0.6	40.9
JG-08	0.2042	.703831	.703540	0.1298	.512817	.512732	4.35	18.315	15.446	38.164	22.94	17.955	15.428	37.676	−0.9	34.2
JG-09	0.2602	.704012	.703641	0.1265	.512802	.512719	4.10	18.235	15.449	38.124	22.47	17.883	15.432	37.659	0.3	41.2
WLHD-01	0.1889	.706071	.705689	0.1196	.512256	.512145	−6.05	17.113	15.303	37.188	9.32	16.905	15.293	36.903	−3.1	83.8
WLHD-02	0.1796	.706037	.705673	0.1113	.512253	.512149	−5.96	17.039	15.277	37.056	5.73	16.911	15.271	36.878	−5.3	80.6
WLHD-03	0.1630	.706086	.705756	0.1243	.512231	.512115	−6.63	17.147	15.312	37.246	9.09	16.944	15.303	36.960	−2.5	84.7
WLHD-04	0.1685	.706118	.705777	0.1142	.512214	.512108	−6.77	17.178	15.311	37.235	9.17	16.973	15.301	36.951	−3.0	80.3
WLHD-05	0.1802	.706073	.705708	0.1095	.512216	.512114	−6.65	17.062	15.301	37.140	6.82	16.910	15.294	36.920	−3.0	85.0
WLHD-06	0.1698	.706130	.705786	0.1186	.512242	.512131	−6.31	16.559	15.230	36.689	9.36	16.350	15.220	36.401	−4.3	100.7
GCS-01	0.4441	.706690	.705840	0.1114	.512128	.512030	−8.49	17.905	15.447	37.853	11.97	17.652	15.435	37.576	3.1	60.8
GCS-02	0.4396	.706728	.705887	0.1115	.512132	.512034	−8.41	17.890	15.448	37.867	13.29	17.609	15.435	37.551	3.5	63.4
GCS-03	0.4239	.706676	.705865	0.1161	.512118	.512016	−8.76	17.920	15.443	37.859	12.45	17.657	15.430	37.553	2.5	57.8
GCS-04	0.4260	.706498	.705683	0.1088	.512115	.512019	−8.69	17.883	15.456	37.869	10.81	17.655	15.445	37.600	4.0	62.9
GCS-05	0.4163	.706657	.705861	0.1086	.512113	.512017	−8.73	17.889	15.439	37.845	12.77	17.620	15.426	37.531	2.5	60.2
GCS-06	0.4486	.706854	.705996	0.1150	.512105	.512004	−9.00	17.889	15.451	37.857	12.39	17.627	15.439	37.563	3.7	62.5
NTS-01	0.2720	.704574	.704185	0.1035	.512671	.512603	1.84	18.050	15.446	38.012	26.36	17.635	15.426	37.433	2.4	48.5
NTS-02	0.2745	.704279	.703886	0.1083	.512667	.512596	1.70	18.015	15.427	37.931	25.43	17.615	15.408	37.399	0.7	47.5
NTS-03	0.2675	.704317	.703934	0.1114	.512733	.512660	2.95	18.018	15.408	37.901	26.81	17.596	15.388	37.327	−1.0	42.7
NTS-04	0.2489	.704360	.704004	0.1076	.512780	.512709	3.92	18.029	15.409	37.931	28.14	17.586	15.388	37.330	−0.9	44.1
NTS-05	0.2285	.704451	.704124	0.1002	.512816	.512750	4.71	18.031	15.419	37.965	25.29	17.633	15.399	37.429	−0.3	48.4
NTS-06	0.2395	.704453	.704110	0.1049	.512664	.512595	1.69	18.000	15.395	37.867	26.96	17.575	15.375	37.285	−2.1	41.0
NTS-07	0.2748	.704406	.704013	0.1017	.512660	.512593	1.65	18.029	15.415	37.922	24.36	17.645	15.396	37.410	−0.7	45.0
NTS-08	0.2263	.704380	.704056	0.1088	.512675	.512603	1.85	18.052	15.433	37.977	28.79	17.599	15.411	37.361	1.2	45.7
NTS-09	0.2682	.704352	.703968	0.1062	.512657	.512587	1.53	18.069	15.434	38.010	26.26	17.655	15.414	37.441	0.9	46.9
FC	0.0324	.709861	.709803	0.0956	.511846	.511767	−13.9	17.733	15.518	37.993	10.76	17.522	15.508	37.551	11.8	74.0

also show slight negative Ti, Nb and Ta anomalies and positive Pb and Sr peaks on spider diagram (Fig. 3f). Their Sr and Nd isotopic compositions fall in a very restricted range (Table 4 and Fig. 4), similar to some of Cenozoic potassic lavas from the Wudalianchi area of Northeastern China (Zhang et al., 1998). Their extremely low ($^{206}Pb/^{204}Pb)_i$ ratios (<17), with prominent positive $\Delta 8/4$ and negative $\Delta 7/4$ values (Table 4), distinguish them from the basalts in the region, but somewhat similar to the Smoky Butte lamproites (Fig. 5a&b) and Wudalianchi potassic rocks (Fig. 5a) (Zhang et al., 1998). The isotopic data, which are compatible with an EM1 source, suggest a long-term evolution in a low-μ environment (low U/Pb and high Th/U ratios).

Guancaishan andesites: The Guancaishan lavas are typical andesites with high SiO_2 (>60 wt.%) and Al_2O_3 (>15.4%) and relatively low alkalis and other oxides (Fig. 2). These lavas are characterized by very low Mg# (<48.5) and low Cr and Ni contents (Table 3), with well-developed negative Eu anomalies (Fig. 3g), indicating that these rocks underwent extensive fractionation of olivine and Ca-plagioclase (±pyroxene). These andesites are enriched in LREE and LILE and depleted in Nb, Ta, Ti, and P (Fig. 3g&h). Like the Wulahada high-Mg andesites, these rocks have very restricted Sr-Nd-Pb isotopic compositions (Table 4 and Figs. 4–5). Their Sr isotope data are similar to those of the Wulahada high-Mg andesites, but the Nd isotope values are more radiogenic.

6. DISCUSSION

6.1. Origin of the Mesozoic Basalts

The geochemical and isotopic compositions of the Mesozoic Jianguo and Niutoushan basalts (Figs. 2–5) are similar to those of the Cenozoic Kuandian and Hannuoba basalts (Zhou and Armstrong, 1982; Peng et al., 1986; Song et al., 1990; Basu et al., 1991; Liu et al., 1995a&b; Barry and Kent, 1998). Both share some common features for modern MORB and OIB and are interpreted as having been derived from the asthenospheric mantle.

The Jianguo basalts have more depleted Sr-Nd isotopic compositions than the Kuandian basalts and plot within the shared field of MORB and OIB (Fig. 4). However, the Pb isotopic compositions are more similar to those of I-MORB or P&N-MORB than those of OIB (Fig. 5a&b). Therefore, the Jianguo basalts were possibly derived from upwelling asthenosphere with a MORB-type isotopic signature. Therefore, their Mg and

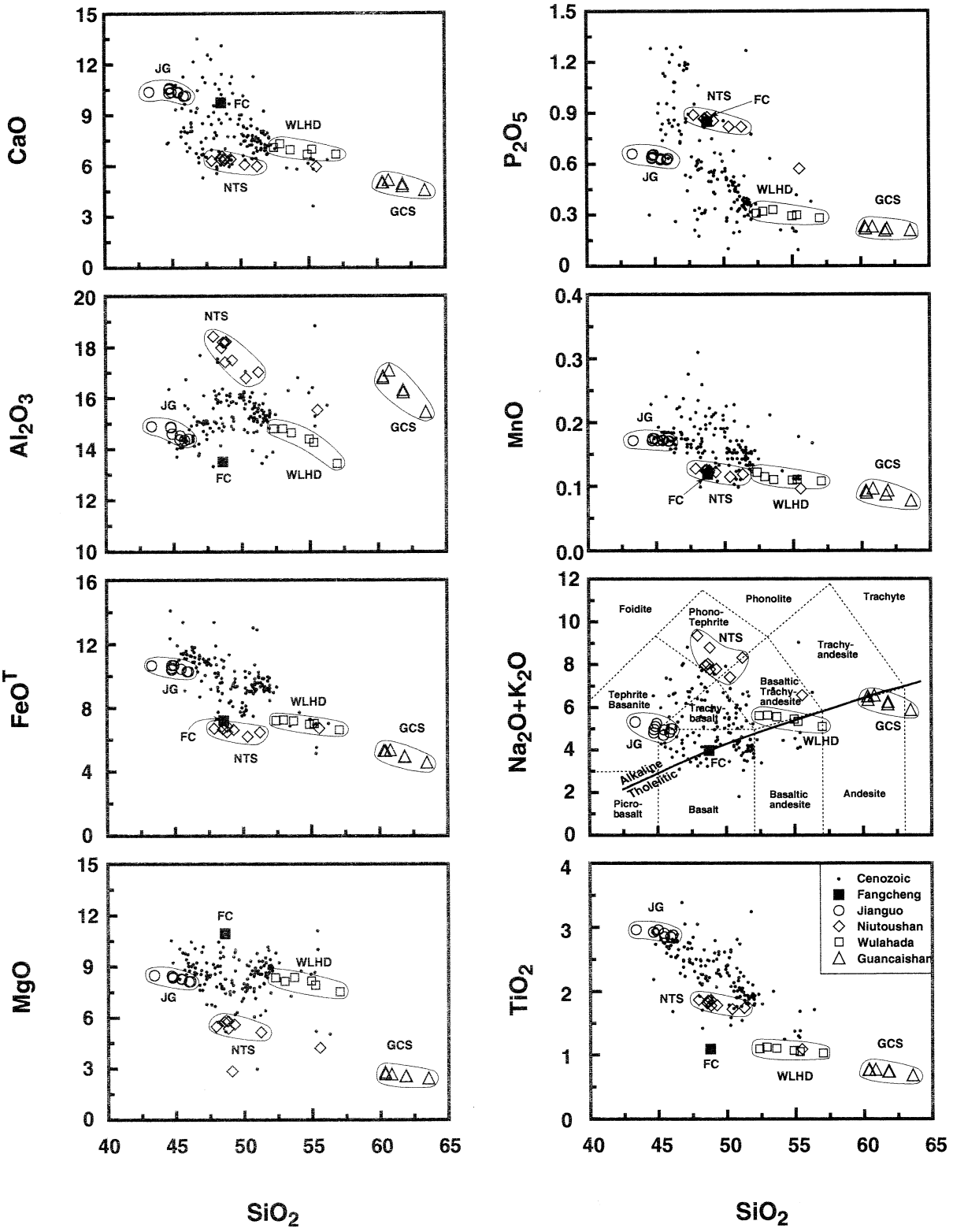

Fig. 2. Major oxide variations in the Mesozoic volcanic lavas, compared with the Cenozoic on-craton basalts and the Mesozoic Fangcheng basalts. Data for the Cenozoic basalts are from Zhou and Armstrong (1982), Peng (1986), Zhi et al. (1990), Basu et al. (1991), Fan and Hooper (1991), Chen (1992), Chen et al. (1992), Fan et al. (1992), and Liu et al. (1995a). Data for the Mesozoic Fangcheng basalts are from Zhang et al. (2002). Classification of volcanic rocks is based on the total alkali-silica diagram of Le Maitre et al. (1989).

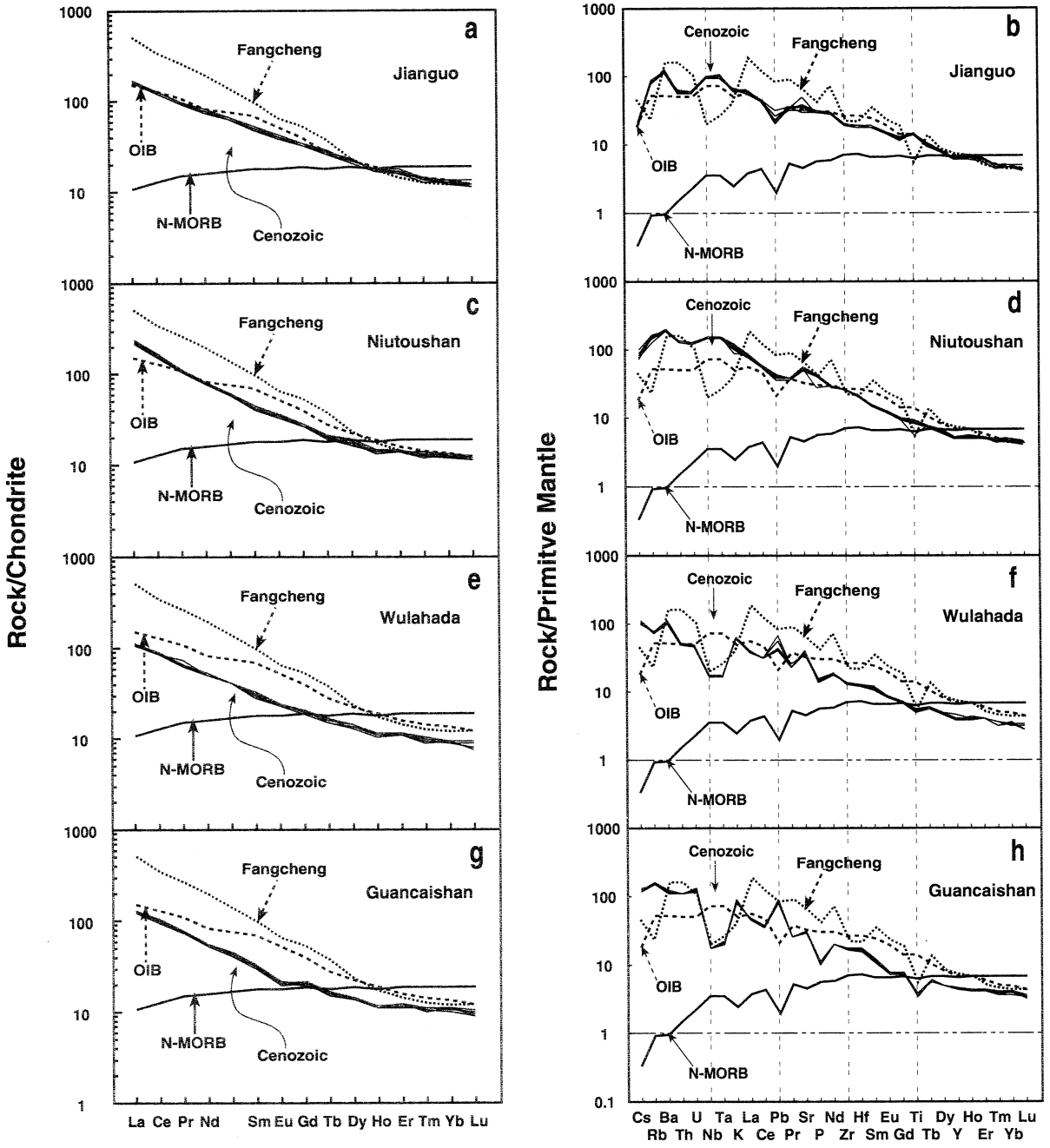

Fig. 3. Chondrite-normalized REE patterns and primitive mantle-normalized trace element diagrams for the Mesozoic volcanic lavas. Normalization values for chondrite and primitive mantle are from McDonough and Sun (1995) and Anders and Grevesse (1989). The shaded field shows the predominant trace element range in Cenozoic on-craton basalts (Zhang et al., 2002). Values for N-MORB, OIB and Fangcheng basalts are from Sun and MacDonough (1989) and Zhang et al. (2002). K, P, and Ti concentrations were calculated from the major oxide contents.

Ni contents and Sr-Nd-Pb isotopic ratios are regarded as a depleted endmembers for modeling calculations in this study.

The Niutoushan basalts have isotopic signatures less depleted than the Jianguo basalts, falling in the OIB field and overlap with the Hannuoba basalts in the Sr-Nd isotopic diagram (Fig. 4). The Pb isotopes overlap with those of I-MORB and the Cenozoic Kuandian and Hannuoba basalts (Fig. 5a&b). These geochemical features suggest a derivation from the asthenosphere, but their very low refractory oxide contents (MgO and NiO) and high alkali contents indicate extensive fractionation of olivine.

6.2. Source for the High-Mg Andesites

High-Mg andesites, as defined by Crawford et al. (1989), represent a group of intermediate rocks with high MgO (>8

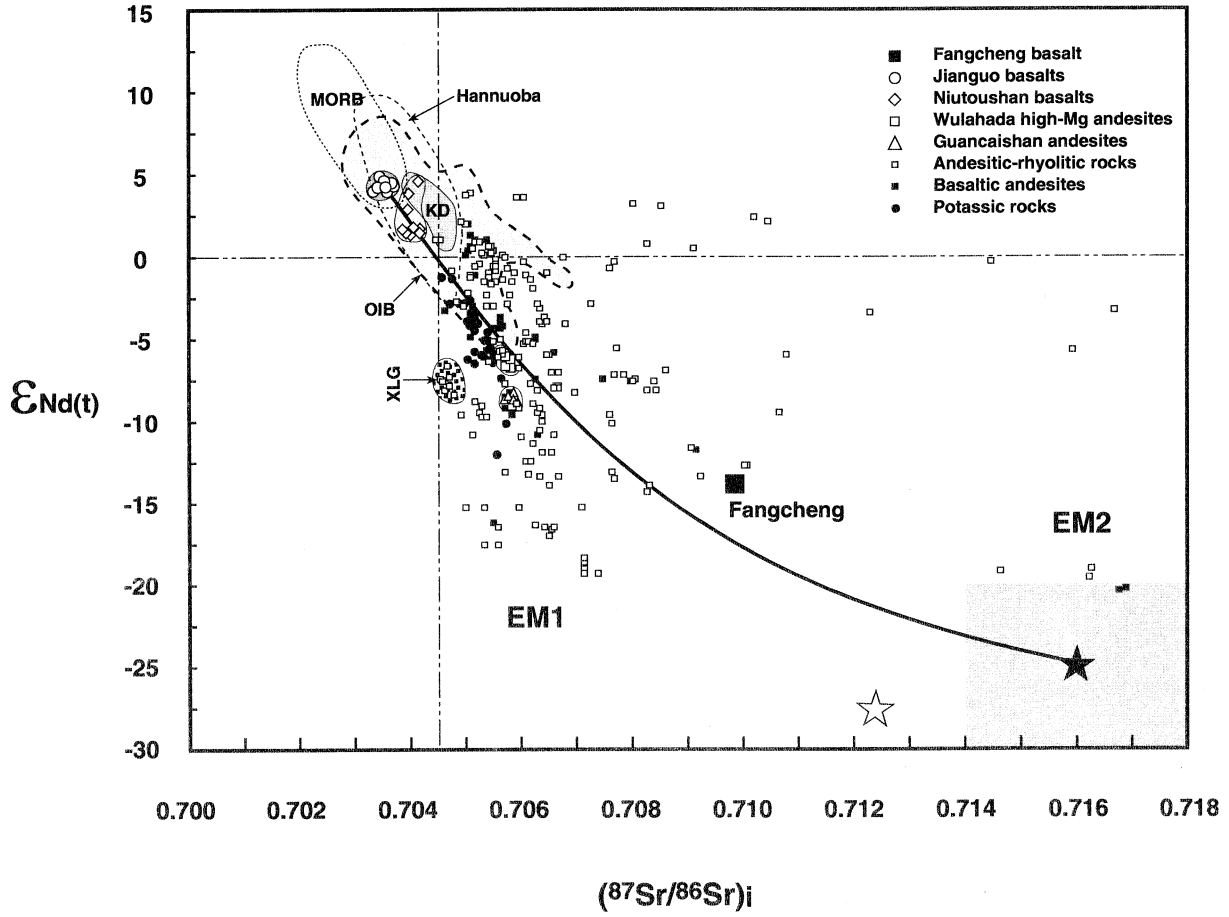

Fig. 4. $(^{87}Sr/^{86}Sr)_i$ vs. ε_{Nd} diagram for the Mesozoic volcanic rocks of the NCC. Data for the Mesozoic Fangcheng and Quaternary Kuandian basalts, including Pb isotopes in Fig. 5, are from Zhang et al. (2002), Zhou and Armstrong (1982), Peng (1986), Basu et al. (1991), Liu et al. (1995b). The MORB, OIB, and Hannuoba field are from Zou et al. (2000), Barry and Kent (1998), and Song et al. (1990). The black star represents the presumed average crustal composition for the NCC ($(^{87}Sr/^{86}Sr)_i \approx 0.716 \pm 0.002$, $\varepsilon_{Nd} \approx -25 \pm 5$ in the Mesozoic) based on isotopic data on Archean crustal terrains (Wu, 1998; Jahn et al., 1999). The white star represents the composition of the old lower crust as represented by a granulite (95SQ10 at 130 Ma, Zhou et al., 2002) from the exposed granulite terrain near Hannuoba. The solid dark line is the mixing trend of depleted MORB mantle (as represented by the Jianguo basalts) with the NCC crust. XLG represents compositions of the basaltic-andesitic lavas from the early Jurassic Xinglonggou Formation (Chen et al., 1999). Also shown are Mesozoic basalts ($SiO_2 < 53\%$, small filled squares) and andesitic-rhyolitic rocks ($SiO_2 > 53\%$, small open squares) based on data from Chen et al. (1997, 1999). The potassic rocks are Cenozoic lavas from the Wudalianchi area of Heilongjiang province in northeastern China (after Zhang et al., 1998).

wt.%) and SiO_2 (>53 wt.% volatile-free) contents (Wang et al., 2002). It is generally believed that two important processes are needed for the generation of these rocks from refractory mantle: (1) a sufficient supply of hydrous components in the refractory mantle to lower the solidus temperature; and (2) a mechanism capable of producing and maintaining a very high geotherm in the mantle wedge (cf. Crawford et al., 1989; Wang et al., 2002). Thus, high-mg andesites are commonly observed in active convergent margins, tectonically mobile belts, or intraplate rifts, and their mantle sources are generally considered to be more refractory than those of MORB (Crawford et al., 1989; Tatsumi and Maruyama, 1989).

The southward subduction of the Paleo-Mongolian Ocean in Paleozoic may modify the northern margin of the NCC, which became the source for the Wulahada high-Mg andesites. The Wulahada High-Mg andesites have moderately high Sr and low Nd isotopic ratios, i.e., EM1 Sr-Nd isotope features (Fig. 4). Their extremely low Pb isotopic ratios (Fig. 5a&b) define a trend toward the field of the Smoky Butte lamproites that are believed to have been derived from an ancient EM1-type subcontinental lithospheric mantle (Fraser et al., 1985). These isotopic features are also similar to those of Cenozoic potassic basalts in northeastern China (Zhang et al., 1998), whose source is interpreted as metasomatically enriched mantle material. Thus, the EM1 geochemical signature of the high-Mg andesites suggests an ancient low-μ mantle source, and their positive $\Delta 8/4$ values (Table 4 and Fig. 5a) suggest derivation from a long-term high Th/U source.

The trace element compositions of these rocks indicate their mantle source is more complex. The incompatible element compositions, such as LILE and LREE (Table 3 and Fig. 3f), are consistent with derivation from an EM1 source. However,

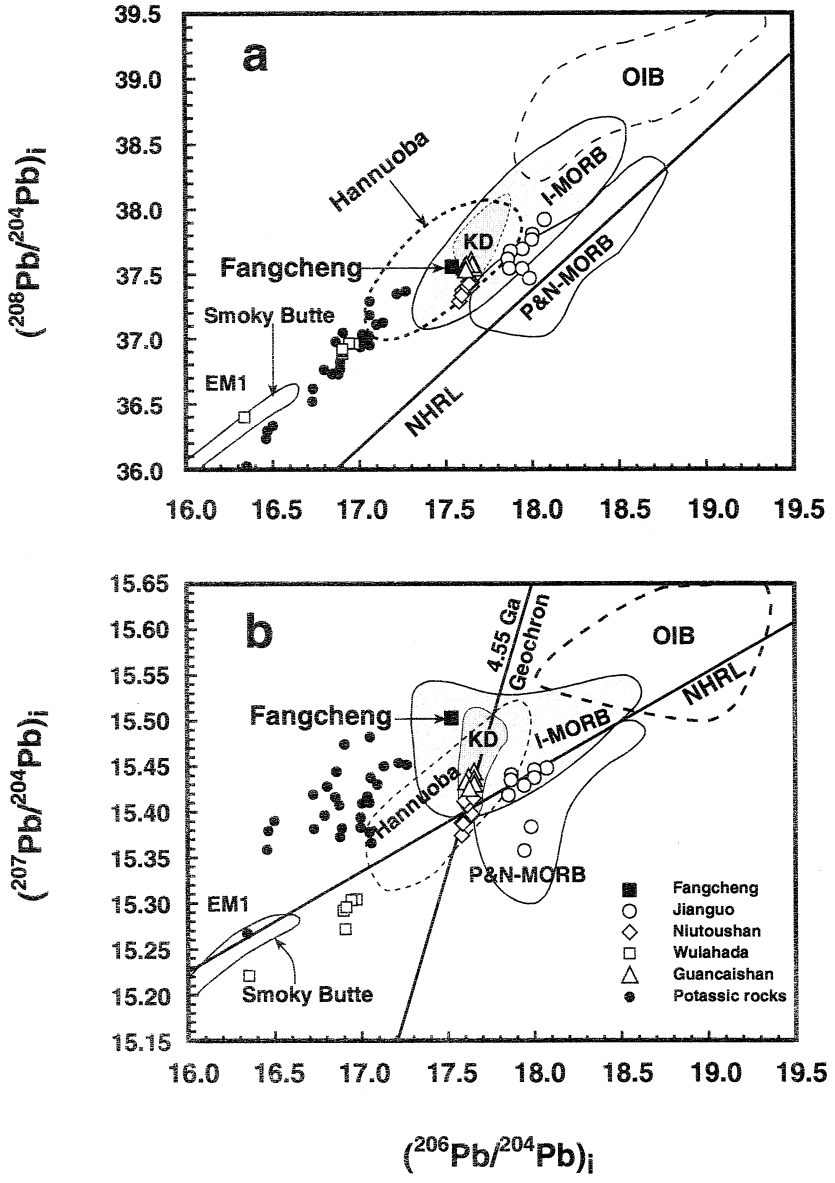

Fig. 5. Initial $^{206}Pb/^{204}Pb$ vs. $^{207}Pb/^{204}Pb$ and $^{208}Pb/^{204}Pb$ diagrams for the Mesozoic volcanic rocks of the NCC. Fields for I-MORB (Most Indian MORB) and P&N-MORB (Pacific and North Atlantic MORB), OIB, and NHRL are taken from Barry and Kent (1998), Zou et al. (2000), and Hart (1984), respectively. Fields for Smoky Butte lamproites and Hannuoba basalts are from Fraser et al. (1985) and Song et al. (1990). Potassic rocks represent Cenozoic lavas from the Wudalianchi area of Heilongjiang province in northeastern China (after Zhang et al., 1998).

obvious depletion of the HFSE (e.g., Nb, Ta, Ti) (Fig. 3f) indicates that the EM1 mantle source must have been previously modified by subduction processes. The high Pb abundances, along with the extremely low Pb isotopic ratios, also suggest a relatively recent addition of subduction-related melts that is possible because Pb is highly soluble in such melts. Thus a refractory lithospheric mantle wedge modified by previous subduction slabs can account for both the incompatible element characteristics and the Sr-Nd-Pb isotopic signatures observed in these high-Mg andesites. Decoupling of the trace element compositions and isotopic ratios indicates that the modification took place relatively recently, so time was insufficient for isotopic evolution. In the NNCC, the most recent tectonic event before the eruption of the high-Mg andesites was Ordovician - Permian southward subduction of the Paleo-Mongolian Ocean and Mesozoic collision between the NCC and the Mongolian block (Robinson et al., 1999; Davis et al., 2001; Buchan et al., 2002). Therefore, we propose that the Wulahada high-Mg basaltic andesites were derived from old refractory lithospheric mantle with an isotopic composition similar to that of EM1 but which was modified by subduction of Paleo-Mongolian oceanic lithosphere. The Mesozoic collision and consequent lithospheric extension triggered decompressional melting of the enriched and highly-modified lithospheric mantle, which produced both high-Mg andesites and high-K, calc-alkaline volcanic rocks of the NNCC.

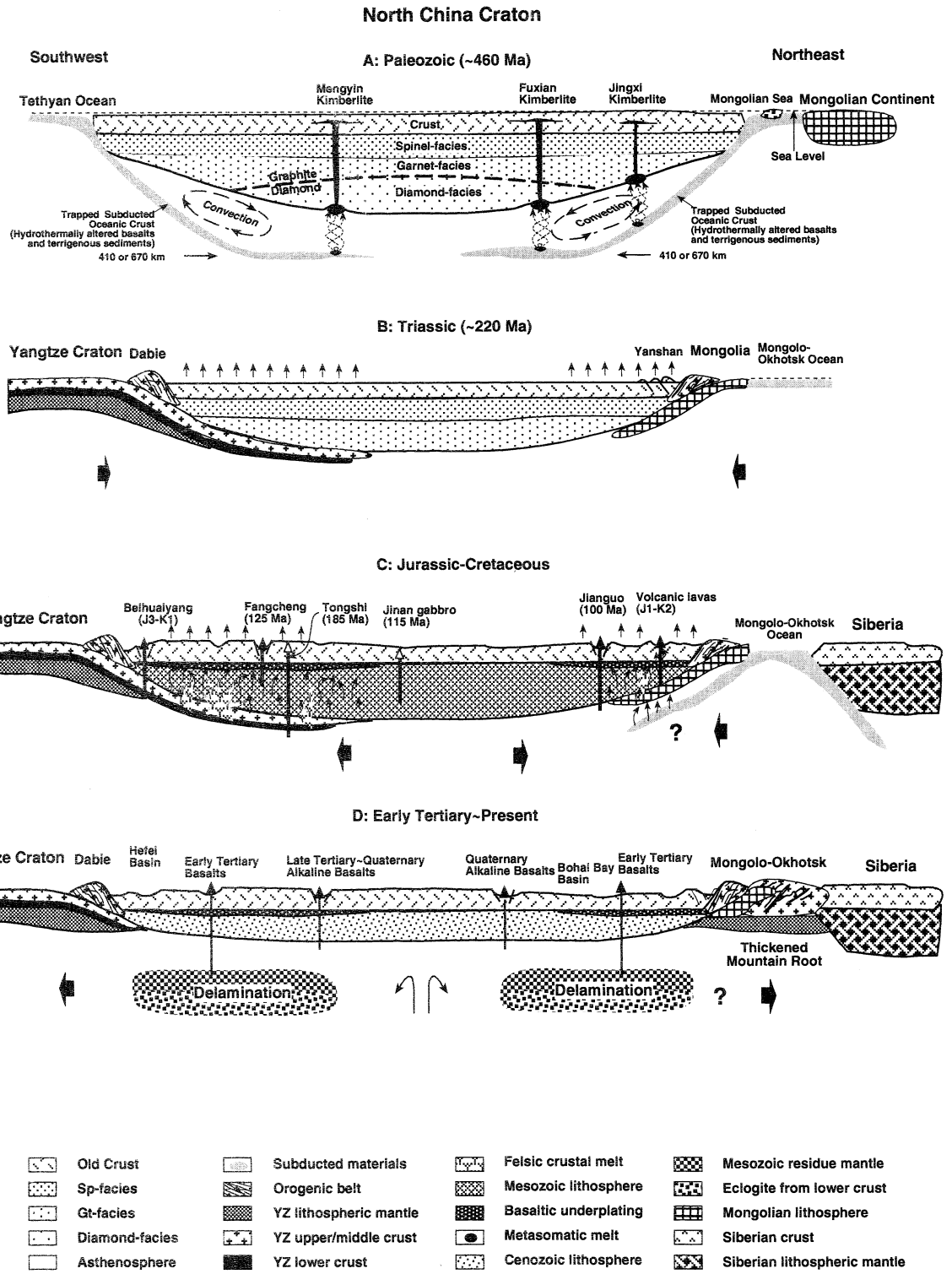
North China Craton
Southwest
A: Paleozoic (~460 Ma)
Northeast
Tethyan Ocean
Mengyin Kimberlite
Fuxian Kimberlite
Jingxi Kimberlite
Mongolian Sea
Mongolian Continent
Crust
Spinel-facies
Garnet-facies
Graphite
Diamond
Diamond-facies
Sea Level
Convection
Convection
Trapped Subducted Oceanic Crust (Hydrothermaliy altered basalts and terrigenous sediments)
410 or 670 km
Trapped Subducted Oceanic Crust (Hydrothermally altered basalts and terrigenous sediments)
410 or 670 km
B: Triassic (~220 Ma)
Yangtze Craton
Dabie
Yanshan
Mongolia
Mongolo-Okhotsk Ocean
C: Jurassic-Cretaceous
Yangtze Craton
Beihuaiyang (J3-K1)
Fangcheng (125 Ma)
Tongshi (185 Ma)
Jinan gabbro (115 Ma)
Jianguo (100 Ma)
Volcanic lavas (J1-K2)
Mongolo-Okhotsk Ocean
Siberia
?
D: Early Tertiary~Present
Yangtze Craton
Dabie
Hefei Basin
Early Tertiary Basalts
Late Tertiary~Quaternary Alkaline Basalts
Quaternary Alkaline Basalts
Bohai Bay Basin
Early Tertiary Basalts
Mongolo-Okhotsk
Siberia
Thickened Mountain Root
Delamination
Delamination
?
Old Crust
Sp-facies
Gt-facies
Diamond-facies
Asthenosphere
Subducted materials
Orogenic belt
YZ lithospheric mantle
YZ upper/middle crust
YZ lower crust
Felsic crustal melt
Mesozoic lithosphere
Basaltic underplating
Metasomatic melt
Cenozoic lithosphere
Mesozoic residue mantle
Eclogite from lower crust
Mongolian lithosphere
Siberian crust
Siberian lithospheric mantle

6.3. Secular Evolution of the Lithosphere under the NCC

To discuss the evolution of the lithospheric mantle beneath the NCC, the nature and thickness of the Paleozoic mantle must first be constrained. There are several Paleozoic kimberlite fields within the NNCC such as Jingxi (Feng et al., 2000) and Tieling (Zhang, 1993) in Liaoning Province. The presence of garnet xenocrysts and garnet peridotite xenoliths in these kimberlites indicates that the lithospheric mantle beneath the region must have been more than 80 km thick before the eruption of the kimberlites. This thickness is much greater than that of the present-day lithosphere beneath the Bohai Sea as revealed by geophysical evidence (cf. Ma, 1987; Griffin et al., 1998). On the other hand, the lack of ultra-high pressure minerals such as diamonds in these kimberlites implies that the lithosphere was less than 150 km thick. Thus, we estimate that the Paleozoic lithosphere of the region was approximately 80 - 150 km thick. Garnets from the Jingxi kimberlites are dominantly Cr-poor and Ca-rich pyropes, suggesting their derivation from a mantle composed of garnet lherzolite (71%), wehrlite (25%), and harzburgite (4%) (Feng et al., 1993). Thus, the Paleozoic lithospheric mantle beneath the Jingxi region was dominantly composed of lherzolite and wehrlite, distinctly different from the highly refractory lithosphere beneath the interior of the craton (up to 50% harzburgite for Mengyin and 30% for Fuxian, Griffin et al., 1998).

The thickness of the Mesozoic lithosphere can be inferred from the geochemical and isotopic compositions of the Mesozoic basalts. Experimental studies show that silica-undersaturated alkaline basalts generally originate from deeper levels than silica-oversaturated tholeiites (Falloon et al., 1988; DePaolo and Daley, 2000). The transition from silica-saturated to undersaturated magmas is controlled by many factors, for instance by the degree of partial melting and the water content. Small degrees of partial melting or low water content will increase the nepheline normative in a melt under a normal geotherm. DePaolo and Daley (2000) suggested that the transition between silica-saturated and undersaturated melts could be as deep as 65 km in the absence of a plume. For a typical continental environment like the NNCC where the initial lithosphere thickness was approximately 80–150 km, the lithosphere- asthenosphere boundary must lie well below this transitional depth. Magmas formed during the first stage of extension should have originated within the lithosphere and therefore have lithospheric isotopic signatures (low ε_{Nd} and high ε_{Sr} values) (DePaolo and Daley, 2000). With continued extension, later lavas could have been derived from the asthenosphere and accordingly possess asthenospheric isotopic signatures. This fits precisely the data for the Mesozoic volcanic rocks of the NNCC; early Jurassic lavas have lithospheric isotopic signatures whereas late Cretaceous lavas show asthenospheric signatures (Fig. 4). Thus, we infer that the alkali basalts with lithospheric isotope signatures were formed when the lithosphere was greater than 80 km thick, and that the tholeiitic and alkali basalts with asthenospheric signatures were derived when the lithosphere was less than 65 km thick. If the basalts have mixed isotopic signatures, the lithosphere is between 65 and 80 km thick (DePaolo and Daley, 2000). Based on this assumption, we suggest that the lithosphere beneath the NNCC was around 65 km thick when the Jianguo basalts were erupted (~100 Ma). This is consistent with the absence of garnet in the mantle xenoliths entrained in the Jianguo basalts (this study and Xu et al., 1999), which suggests that the lithospheric mantle in the late Cretaceous was composed predominantly of spinel lherzolite with numerous pyroxenite veins or dikes. The presence of metasomatic pargasite and plagioclase-bearing pyroxenite in the mantle xenoliths indicates that high silica melts percolated through the Paleozoic lithosphere as demonstrated for the SNCC (Zhang et al., 2002) and other cratons worldwide (Pilet et al., 2002). We conclude that the lithosphere in this region was not only thinned by extension but also became more fertile as extension proceeded.

Detailed mineralogical investigations of the Mesozoic xenoliths (Xu et al., 1999) reveal that the compositions of olivine (Fo=89.3–91.5), orthopyroxene, clinopyroxene, and spinel are similar to those in mantle xenoliths entrained in the adjacent Quaternary and Tertiary basalts in eastern China (Fang and Ma, 1999; Fan et al., 2000). Based on the similarity in mineral assemblage and compositions, we infer that the lithospheric mantle in the region had developed its well-defined “oceanic” character by the late Cretaceous (Fan et al., 2000). This implies that the lithospheric thinning and replacement occurred much earlier on the northern margin of the NCC than on the southern margin, because there is no evidence of such a thin lithosphere in the southern portion, as indicated by 125 Ma Fangcheng

Fig. 6. Schematic sections through the NCC illustrating reactivation of the eastern NCC, transformation of the old cratonic lithosphere to the Mesozoic fertile lithosphere, and lithospheric thinning as a result of postorogenic lithospheric extension and eruption of magma (refined from Zhang et al., 2002 and Zhang and Sun, 2002). (A) Paleozoic northward subduction of the Proto-Tethyan ocean and southward subduction of the Mongolian ocean beneath the well-stratified cratonic lithosphere induced dehydration melting of the subducted crust (hydrothermaly-altered basalts and terrigenous sediments), which produced high-K melts. Migration of these melts initiated partial melting of the lowermost lithosphere and the uppermost asthenosphere to produce kimberlites; (B) Triassic collision of the Yangtze craton and the Mongolian microcontinent with the NCC triggered destruction of the NCC lithosphere, simultaneously with the formation of the Dabie orogenic belt, the Central Asia orogenic belt, and the Yanshan fold and thrust belt. Tectonic underplating of the Yangtze and Mongolian crust beneath the NCC lithosphere uplifted the both sides of the NCC; (C) after the 30–50 Ma the subducted continental slab produced silicic melts, which modified the overlying refractory lithospheric mantle. Continuous modification by these melts converted the old cratonic lithospheric mantle to Mesozoic enriched lithospheric mantle. Postorogenic lithospheric extension caused decompressional melting of the enriched lithosphere during the Jurassic-Cretaceous time, producing voluminous high-Mg basaltic andesites and high-K calc-alkali volcanic rocks. Basaltic magma was underplated at the base of the crust, forming newly-accreted lower crust; (D). Eclogitization of the residue root and delamination of the eclogites together with the overriding residue mantle in the late Cretaceous or early Tertiary. Crystallization of the uprising asthenosphere led to formation of the Cenozoic fertile lithospheric mantle. The presence of slightly enriched mafic rocks in the center and highly isotopically enriched rocks on both sides of the NCC support this geodynamic model.

basalts (Zhang et al., 2002). Furthermore, the Quaternary Kuandian basalts are richer in alkalis than the nearby Jianguo basalts (Table 2), implying a greater depth to the lithosphere-asthenosphere boundary in the Quaternary. This is consistent with the occurrence of garnet as megacrysts or in garnet pyroxenite xenoliths in the Kuandian basalts (Fang and Ma, 1999). However, garnet is only a minor phase in these xenoliths, which consist of spinel-facies lherzolite, harzburgite and pyroxenite, not garnet peridotite (Fang and Ma, 1999; Song and Frey, 1989; Tatsumoto et al., 1992). This demonstrates that the Cenozoic lithosphere was thinner than 80 km, consistent with geophysical evidence pointing to a thin, present-day lithosphere beneath the eastern NCC (Ma, 1987; Griffin et al., 1998; Poudjom Djomani et al., 2001). The ubiquitous occurrence of coarse-grained harzburgite and the scarcity of metasomatic amphibole in the mantle xenoliths from the Cenozoic basalts illustrate the compositional differences between the Cenozoic and the late Mesozoic lithospheric mantle. The newly-accreted lithosphere probably was predominantly refractory harzburgite. It should be noted that coarse-grained harzburgite could also be produced by asthenosphere-lithosphere interaction (Xu et al., 1998). Finally, during a late stage of extension, thermal relaxation produced subsidence around the Bohai Sea, where the lithosphere is currently the thinnest in eastern China (Griffin et al., 1998; Ren et al., 2002).

In summary, the enriched Mesozoic lithospheric mantle evolved from a refractory Paleozoic lithospheric mantle by the addition of melt from old, subducted continental crust. The Mesozoic mantle lithosphere then was transformed into the Cenozoic oceanic lithospheric mantle by accretion. Beneath the NNCC, the 80~150-km-thick Paleozoic lithosphere was gradually thinned to about 65 km in the late Cretaceous in response to postcollisional lithospheric extension and further reached a thickness of about 80 km in the Quaternary with the lithospheric accretion.

6.4. Mechanism of Lithosphere Thinning

It is widely accepted that the lithospheric mantle beneath the eastern NCC has been thinned considerably since the Phanerozoic, as evidenced by geophysical and geochemical data. More importantly, the nature of lithospheric mantle has changed from refractory, buoyant Archean material to fertile, less buoyant Cenozoic material (Griffin et al., 1992, 1998; Menzies et al., 1993; Menzies and Xu, 1998; Fan et al., 2000; O'Reilly et al., 2001; Poudjom Djomani et al., 2001; Zheng et al., 2001). However, the mechanism responsible for the thinning and change in composition is still unclear. Many authors (Griffin et al., 1998; Zheng 1999; Zheng et al., 2001; O'Reilly et al., 2001; Poudjom Djomani et al., 2001) believe that the changes probably involved mechanical dispersal by rifting, accompanied by the rise of hot, fertile asthenospheric material. The presence of both high- and low-magnesian olivine in spinel-facies peridotitic xenoliths entrained in the Hebi Cenozoic basalts (Zheng et al., 2001) provides some evidence for such a process. More convincing evidence comes from newly published Os isotopic data (Wu et al., 2003) on peridotite xenoliths in the Cenozoic basalts of the NNCC. Extremely young Re depletion model ages for these peridotites suggest the removal of the Archean cratonic lithospheric mantle and the addition of much younger, lithospheric mantle. In contrast, others (Menzies and Xu, 1998; Xu, 2001) have emphasized the importance of thermo-chemical erosion resulting from upwelling of hot asthenosphere. However, these models are not supported by the data available on the Mesozoic lavas and mantle xenoliths.

The geochemistry of Mesozoic basalts from Fangcheng on the SNCC can best be explained by addition of silicic melts to the source region (Zhang et al., 2002; Zhang and Sun, 2002). This addition was accomplished by the introduction of melts from subducted Yangtze crust into the old refractory lithospheric mantle after the collision between the NCC and the Yangtze craton in Triassic. A northward decrease in enrichment of the mafic volcanic rocks (Zhang and Sun, 2002) demonstrates that late Mesozoic lithospheric replacement was related to deep subduction and collision along the Dabie-Sulu orogenic belt, which led to a major change in the composition and thermal state of the lithosphere in the region, and finally resulted in the transformation of the Archean refractory lithospheric mantle to the late Mesozoic fertile lithospheric mantle. Thus, interaction between slab-related melts and refractory lithosphere is considered an important process in the lithosphere replacement.

In the NNCC, the occurrence of high-Mg andesites also demonstrates interaction of slab-derived melts with refractory lithosphere. Voluminous mafic-silicic volcanism in the early Jurassic - late Cretaceous (Chen et al., 1997) indicates that lithosphere thinning on the NNCC occurred much earlier than on the SNCC where volcanism occurred only in the Cretaceous (~120 Ma). The discovery of altered oceanic crustal components in garnet pyroxenite and mafic granulite xenoliths contained in the Hannuoba basalt (Xu, 2002) provide further evidence for interaction between the lithosphere and slab-derived melts.

We present a geodynamic model in Figure 6, suggesting that subduction of oceanic crust beneath both the northern and southern margins of the NCC in the Paleozoic (Meng and Zhang, 2000; Davis et al., 2001, Ren et al., 2002) was responsible for destabilization of the eastern NCC and the resulting thinning and replacement of the lithospheric mantle. Destruction of the lithosphere in this region continued during Mesozoic continental subduction and continent-continent collision. Interaction between the refractory lithospheric mantle and slab-derived silicic melts led to the formation of the young fertile lithospheric mantle from which the Mesozoic mafic volcanic rocks were derived. The replacement took place predominantly in Cretaceous time. This fertile Mesozoic mantle was then replaced by oceanic lithospheric mantle in the Cenozoic (Fan et al., 2000), probably by delamination of the subcontinental lithospheric mantle (Poudjom Djomani et al., 2001) and accretion of the upwelling asthenospheric materials.

7. CONCLUSIONS

Integrated elemental and Sr-Nd-Pb isotopic studies of the Mesozoic basalts and high-Mg andesites on the eastern NCC allow us to reach the following conclusions:

(1) Basalts from the NNCC contrast markedly with those from the SNCC and have MORB-type Sr-Nd-Pb isotope signature indicative of derivation from upwelling asthenosphere.

(2) High-Mg andesites from the NNCC have decoupled elemental and isotopic compositions (EM1-type), suggesting a long-term evolved lithospheric mantle source modified considerably by a slab-derived melt. This subduction-related modification of the old refractory lithospheric mantle provides a mechanism for the observed thinning and replacement of the lithosphere.

(3) Secular evolution of Mesozoic lithospheric mantle beneath the eastern NCC is apparent with thicker, less modified lithospheric mantle in the interior and thinner, more heavily modified lithospheric mantle beneath craton margins. The cratonic lithospheric mantle was progressively transformed into fertile lithospheric mantle (peridotites + pyroxenites) through the massive addition of slab-derived melts in the Mesozoic.

Acknowledgments—This research was financially supported by Chinese Academy of Sciences (KZCX1-07, KZCX3-SW-135), the National Science Foundation of China (40225009), Hong Kong RGC grant (HKU7115/00P) and an award from the University of Hong Kong. Paul Robinson is appreciated for the comments on the early version of the manuscript. M.A. Menzies, Y.G. Xu, R.L. Rudnick and an anonymous reviewer are thanked for the constructive reviews that improved the paper considerably.

Associate editor: M. A. Menzies

REFERENCES

Anders E. and Grevesse N. (1989) Abundances of the elements: Meteoritic and solar. *Geochim. Cosmochim. Acta* **53,** 197–214.

Barry T. L. and Kent R. W. (1998) Cenozoic magmatism in Mongolia and the origin of central and east Asian basalts. In *Mantle Dynamics and Plate Interactions in East Asia* (eds. M. F. J. Flower, S. L. Chung, C. H. Lo, and T. Y. Lee), pp. 347–364. American Geophysical Union, Geodynamics Series 27.

Basu A. R., Wang J. W., Huang W. K., Xie G. H., and Tatsumoto M. (1991) Major element, REE and Pb, Nd and Sr isotopic geochemistry of Cenozoic volcanic rocks of eastern China: Implications for origin from suboceanic-type mantle reservoirs. *Earth Planet. Sci. Lett.* **105,** 149–169.

Buchan C., Pfänder J., Kröner A., Brewer T. S., Tomurtogoo O., Tomurhuu D., Cunningham D., and Windley B. F. (2002) Timing of accretion and collisional deformation in the Central Asian Orogenic Belt: Implications of granite geochronology in the Bayankhongor ophiolite zone. *Chem. Geol.* **192,** 23–45.

Chen D. G. (1992) Geochemistry of Cenozoic basalts from the middle-southern part of Tan-Lu faults (in Chinese). In *Chronology and Geochemistry of Cenozoic Basalts in China* (ed. R. X. Liu), pp. 171–200. The Seismological Press, Beijing.

Chen W. J., Li D. M., Li Q., Sheng S. W., Liang H. D., Zhou X. H., Liu R. X., Wang X., Liu X. T., and Zheng J. W. (1992) Geochronology and geochemistry of basalts from Xialiaohe rift basin (in Chinese). In *Chronology and Geochemistry of Cenozoic Basalts in China* (ed. R. X. Liu), pp. 44–80. The Seismological Press, Beijing.

Chen W. J., Zhou X. H., Li Q., Yang J. H., Li D. M., Chen S. H., Zheng D. W., Wan J. Q., Zhang G. H., and Wang F. (1999) *Research on Mesozoic volcanic chronology, geochemistry and tectonic settings around the Liaohe River* (in Chinese). Internal report of the Institute of Geology, Seismological Bureau of China.

Chen Y. X., Chen W. J., Zhou X. H., Li Z. J., Liang H. D., Li Q., Xu K., Fan Q. C., Zhang G. H., Wang F., Wang Y., Zhou S. Q., Chen S. H., Hu B., and Wang Q. J. (1997) *Liaoxi and Adjacent Mesozoic Volcanics-Chronology, Geochemistry and Tectonic Settings* (in Chinese). The Seismological Press, Beijing.

Crawford A. J., Falloon T. J., and Green D. H. (1989) Classification, petrogenesis and tectonic setting of boninites. In *Boninites* (ed. A. J. Crawford), pp. 1–49. Unwin Hyman, London.

Davis G., Zheng Y. D., Wang C., Darby B. J., Zhang C. H., and Gehrels G. (2001) Mesozoic tectonic evolution of the Yangshan fold and thrust belt, with emphasis on Hebei and Liaoning provinces, northern China. In *Paleozoic and Mesozoic Tectonic Evolution of Central Asia: From Continental Assembly to Intracontinental Deformation* (eds. H. S. Hendrix and G. A. Davis), pp. 171–197. Boulder Colorado, Geological Society of America Memoir 194.

DePaolo D. J. and Daley E. E. (2000) Neodymium isotopes in basalts of the southwest basin and range and the lithospheric thinning during continental extension. *Chem. Geol.* **169,** 157–185.

Falloon T. J., Green D. H., Harton C. J., and Harris K. J. (1988) Anhydrous partial melting of a fertile and depleted peridotite from 2 to 30 kb and application to basalt petrogenesis. *J. Petrol.* **29,** 1257–1282.

Fan Q. and Hooper P. R. (1991) The Cenozoic basaltic rocks of Eastern China: Petrology and chemical composition. *J. Petrol.* **32,** 765–810.

Fan Q. C., Chen W. J., Hurford A. J., and Hunziker J. G. (1992) Major and trace element geochemistry of Datong basalts (in Chinese). In *Chronology and Geochemistry of Cenozoic Basalts in China* (ed. R. X. Liu), pp. 93–100. The Seismological Press, Beijing.

Fan W. M., Zhang H. F., Baker J., Jarvis K. E., Mason P. R. D., and Menzies M. A. (2000) On and off the North China Craton: Where is the Archaean keel? *J. Petrol.* **41,** 933–950.

Fan W. M., Guo F., Wang Y. J., Lin G., and Zhang M. (2001) Post-orogenic bimodal volcanism along the Sulu orogenic belt in eastern China. *Phys. Chem. Earth (A)* **26,** 733–746.

Fang X. H. and Ma H. W. (1999) Lithospheric mantle composition and thermal structure beneath Kuandian, Liaoning Province - information from mantle xenoliths (in Chinese). *Geol. Rev.* **45** (suppl)**,** 450–457.

Feng C., Zhang H.-F., and Zhou X. H. (1993) New kimberlite field found in Liaoxi, China (in Chinese). *Seismological Geol.* **22**(suppl.)**,** 95–98.

Fraser K. J., Hawkesworth C. J., Erland A. J., Mitchell R. H., and Scott-Smith B. H. (1985) Sr, Nd and Pb isotope and minor element geochemistry of lamproites and kimberlites. *Earth Planet. Sci. Lett.* **76,** 57–70.

Gao S., Rudnick R., Carlson R. W., McDonough W. F., and Liu Y. S. (2002) Re-Os evidence for replacement of ancient mantle lithosphere beneath the North China craton. *Earth Planet. Sci. Lett.* **198,** 307–322.

Griffin W. L., O'Reilly S. Y., and Ryan C. G. (1992) Composition and thermal structure of the lithosphere beneath south Africa, Siberia and China: Proton microprobe studies. *Abstract of International Symposium on Cenozoic volcanic rocks and deep-seated xenoliths of China and its environs.* Beijing, pp. 65–66.

Griffin W. L., Zhang A. D., O'Reilly S. Y., and Ryan C. G. (1998) Phanerozoic evolution of the lithosphere beneath the Sino-Korean Craton. In *Mantle Dynamics and Plate Interactions in East Asia* (eds. M. F. J. Flower, S. L. Chung, C. H. Lo, and T. Y. Lee), pp. 107–126. American Geophysical Union, Geodynamics Series 27.

Hart S. R. (1984) A large-scale isotope anomaly in the Southern Hemisphere mantle. *Nature* **309,** 753–757.

Jahn B. M., Wu F. Y., Lo C. H., and Tsai C. H. (1999) Crust-mantle interaction induced by deep subduction of the continental crust: Geochemical and Sr-Nd isotopic evidence from post-collisional mafic-ultramafic intrusions of the northern Dabie complex, central China. *Chem. Geol.* **157,** 119–146.

Le Maitre R. W., Bateman P., Dubek A., Keller J., Lameyre J., Le Bas M. J., Sabine P. A., Schimid R., and Sorensen H. (1989) *A Classification of Igneous Rocks and Glossary of Terms: Recommendations of the Inter-national Union of Geological Sciences Subcommission on the Systematics of Igneous Rocks*. Blackwell, Oxford.

Li S. G., Xiao Y. L., Liou D. L., Chen Y. Z., Ge N. J., Zhang Z. Q., Sun S. S., Cong B. L., Zhang R. Y., Hart S. R., and Wang S. S. (1993) Collision of the North China and Yangtze Blocks and formation of coesite-bearing eclogites - Timing and processes. *Chem. Geol.* **109,** 89–111.

Li X. H., Liu Y., Tu X. L., Hu G. Q., and Zeng W. (2002) Precise determination of chemical compositions in silicate rocks using ICP-AES and ICP-MS: A comparative study of sample digestion techniques of alkali fusion and acid dissolution (in Chinese). *Geochemica* **31**(3)**,** 289–294.

Liu C. Q., Xie G. H., and Masuda A. (1995a) Geochemistry of Cenozoic basalts from eastern China - I. Major element and trace element compositions: Petrogenesis and characteristics of mantle source (in Chinese). *Geochemistry* **24**(1)**,** 1–19.

Liu C. Q., Xie G. H., and Masuda A. (1995b) Geochemistry of Cenozoic basalts from eastern China - II. Sr, Nd and Ce isotopic compositions (in Chinese). *Geochemistry* **24**(3)**,** 203–213.

Liu J. B., Ye K., Maruyama S., Cong B. L., and Fan H. R. (2001) Mineral inclusions in zircon from gneisses in the ultrahigh-pressure zone of the Dabie Mountains, China. *J. Geol.* **109,** 523–535.

Lugmair G. W. and Marti K. (1978) Lunar initial $^{143}Nd/^{144}Nd$: Differential evolution of the lunar crust and mantle. *Earth Planet. Sci. Lett.* **39,** 349–357.

Ma X. Y (1987) *Lithospheric Dynamics Map of China and Adjacent Seas (1:4,000,000) and Explanatory Notes.* Geological Publishing House, Beijing.

McDonough W. F. and Sun S. S. (1995) The composition of the Earth. *Chem. Geol.* **120,** 223–253.

Meng Q. R. and Zhang G. W. (2000) Geologic framework and tectonic evolution of the qinling orogen, central China. *Tectonophysics* **323,** 183–196.

Menzies M. A. and Xu Y. G. (1998) Geodynamics of the North China Craton. In *Mantle Dynamics and Plate Interactions in East Asia* (eds. M. F. J. Flower, S. L. Chung, C. H. Lo, and T. Y. Lee), pp. 155–165. American Geophysical Union, Geodynamics Series 27.

Menzies M. A., Fan W. M., and Zhang M. (1993) Palaeozoic and Cenozoic lithoprobes and the loss of >120 km of Archaean lithosphere, Sino-Korean craton, China. In *Magmatic Processes and Plate Tectonics* (eds. H. M. Prichard, T. Alabaster, N. B. W. Harris, and C. R. Neary), pp. 71–78. Geol. Soc. Special Pub. 76.

O'Reilly S. Y., Griffin W. L., Poudjom Djomani Y. H., and Morgan P. (2001) Are lithospheres forever? Tracking changes in sub-continental lithospheric mantle through time. *GSA Today* **11**(4)**,** 4–10.

Peng Z. C., Zartman R. E., Futa E., and Chen D. G. (1986) Pb-, Sr- and Nd-isotopic systematics and chemical characteristics of Cenozoic basalts, eastern China. *Chem. Geol.* **59,** 3–33.

Pilet S., Hernandez J., and Villemant B. (2002) Evidence for high silicic melt circulation and metasomatic events in the mantle beneath alkaline provinces: The Na-Fe-augitic green-core pyroxenes in the Tertiary alkali basalts of the Cantal massif (French Massif Central). *Mineral. Petrol.* **76,** 39–62.

Poudjom Djomani Y. H., O'Reilly S. Y., Griffin W. L., and Morgan P. (2001) The density structure of subcontinental lithosphere through time. *Earth Planet. Sci. Lett.* **184,** 605–621.

Qi L., Hu J., and Gregoire D. C. (2000) Determination of trace elements in granites by inductively coupled plasma mass spectrometry. *Talanta* **51,** 507–513.

Ren J. Y., Tamaki K., Li S. T., and Zhang J. X. (2002) Late Mesozoic and Cenozoic rifting and its dynamics setting in eastern China and adjacent areas. *Tectonophysics* **344,** 175–205.

Robinson P. T., Zhou M. F., Hu X. F., Reynolds P., Bai W. J., and Yang J. S. (1999) Geochemical constraints on the origin of the Hegenshan ophiolite, Inner Mongolia, China. *J. Asian Earth Sci.* **17,** 423–442.

Şengör A. M. C., Natal'in B. A., and Burtman V. S. (1999) Evolution of the altaid tectonic collage and Palaeozoic crustal growth in Eurasia. *Nature* **364,** 299–307.

Song Y. and Frey F. A. (1989) Geochemistry of peridotite xenoliths in basalt from Hannuoba, eastern China: Implications for subcontinental mantle heterogeneity. *Geochim. Cosmochim. Acta* **53,** 97–113.

Song Y., Frey F. A., and Zhi X. C. (1990) Isotopic characteristics of Hannuoba basalts, eastern China: Implications for their petrogenesis and the composition of subcontinental mantle. *Chem. Geol.* **85,** 35–52.

Steiger R. H. and Jäger E. (1977) Subcommission on geochronology; convention on the use of decay constants in geochronology and cosmochronology. *Earth Planet. Sci. Lett.* **36,** 359–362.

Sun S. S. and McDonough W. F. (1989) Chemical and isotopic systematics of oceanic basalts: Implications for mantle composition and processes. In *Magmatism in the Ocean Basins* (eds. A. D. Saunders and M. J. Norry), pp. 313–345. Geol. Soc. Special Pub..

Tatsumi Y. and Maruyama S. (1989) Boninites and high-Mg andesites: Tectonics and petrogenesis. In *Boninites* (ed. A. J. Crawford), pp. 50–71. Unwin Hyman, London.

Tatsumoto M., Basu A. R., Huang W. K., Wang J. W., and Xie G. H. (1992) Sr, Nd, and Pb isotopes of ultramafic xenoliths in volcanic rocks of Eastern China: Enriched components EMI and EMII in subcontinental lithosphere. *Earth Planet. Sci. Lett.* **113,** 107–128.

Wang K. L., Chung S. L., Chen C. H., and Chen C. H. (2002) Geochemical constraints on the petrogenesis of high-Mg basaltic andesites from the Northern Taiwan Volcanic Zone. *Chem. Geol.* **182,** 513–528.

Wu F. Y. (1998) Age and accretionary process of the continental crust. In *Chemical Geodynamics* (ed. Y. F. Zheng), pp. 224–261. Scientific Press, Beijing.

Wu F. Y., Walker R. J., Ren X. W., Sun D. Y., and Zhou X. H. (2003) Osmium isotopic constraints on the age of lithospheric mantle beneath northeastern China. *Chem. Geol.* **14156,** 1–23.

Xu B. and Chen B. (1997) Framework and evolution of the middle Paleozoic orogenic belt Siberian and North China Plates in northern Inner Mongolia. *Sci. in China (D)* **40,** 463–479.

Xu S. T., Okay A. J., Ji S., Sengör A. M. C., Su W., Liu Y., and Jiang, L. (1992) Diamond from Dabie Shan metamorphic rocks and its implication for tectonic setting. *Science* **256,** 80–82.

Xu W. L., Zheng C. Q., and Wang D. Y. (1999) Discovery of the mantle and lower crust xenoliths in Mesozoic trachy-basalts in Liaoxi, China and its significance (in Chinese). *Geol. Rev.* **45**(suppl)**,** 444–449.

Xu Y. G. (2001) Thermo-tectonic destruction of the Archean lithospheric keel beneath the Sino-Korean Craton in China: Evidence, timing and mechanism. *Phys. Chem. Earth (A)* **26,** 747–757.

Xu Y. G. (2002) Evidence for crustal components in the mantle and constraints on crustal recycling mechanism: Pyroxenite xenoliths from Hannuoba, North China. *Chem. Geol.* **182,** 301–322.

Xu Y. G., Menzies M. A., Vroon P., Mercier J. C., and Lin C. Y. (1998) Texture-temperature- geochemistry relationship in the upper mantle as revealed from spine1 peridotite xenoliths from Wangqing, NE China. *J. Petrol.* **39,** 469–493.

Ye K., Cong B. L., and Ye D. N. (2000) The possible subduction of continental material to depths greater than 200 km. *Nature* **407,** 734–736.

Zhang H.-F. (1993) Preliminary study on the geochemical characteristics and petrogenesis of the Tieling kimberlites, Liaoning Province (in Chinese). *Modern Geol.* **7**(4)**,** 458–464.

Zhang H.-F. and Sun M. (2002) Geochemistry of Mesozoic basalts and mafic dikes in southeastern North China craton, and tectonic implication. *Int. Geol. Rev.* **44,** 370–382.

Zhang H.-F., Sun M., Zhou X. H., Fan W. M., Zhai M. G., and Yin J. F. (2002) Mesozoic lithosphere destruction beneath the North China Craton: Evidence from major, trace element, and Sr-Nd-Pb isotope studies of Fangcheng basalts. *Contrib. Mineral. Petrol.* **144,** 241–253.

Zhang M., Zhou X. H., and Zhang J. B. (1998) Nature of the lithospheric mantle beneath NE China: Evidence from potassic volcanic rocks and mantle xenoliths. In *Mantle Dynamics and Plate Interactions in East Asia* (eds. M. F. J. Flower, S. L. Chung, C. H. Lo, and T. Y. Lee), pp. 197–219. American Geophysical Union, Geodynamics Series 27.

Zhao G. C., Wilde S. A., Cawood P. A., and Sun M. (2002) SHRIMP U-Pb zircon ages of the Fuping complexes: Implications for late Archean to Paleoproterozoic accretion and assembly of the North China Craton. *Am. J. Sci.* **302,** 191–226.

Zheng J. P. (1999) Mesozoic–Cenozoic Mantle Replacement and Lithospheric Thinning, East China (in Chinese with English abstract). University of Geosciences Press, China.

Zheng J. P., O'Reilly S. Y., Griffin W. L., Lu F. X., Zhang M., and Pearson N. J. (2001) Relict refractory mantle beneath the eastern North China block: Significance for lithosphere evolution. *Lithos* **57,** 43–66.

Zhi X., Song Y., Frey F. A., Feng J., and Zhai M. (1990) Geochemistry of Hannuoba basalts, eastern China: Constraints on the origin of continental alkali and tholeiitic basalt. *Chem. Geol.* **88,** 1–33.

Zhou X. H. and Armstrong R. L. (1982) Cenozoic volcanic rocks of eastern China - Secular and geographic trends in chemistry and strontium isotopic composition. *Earth Planet. Sci. Lett.* **59,** 301–329.

Zhou X. H., Sun M., Zhang G. H., and Chen S. H. (2002) Continental crust and lithospheric mantle interaction between North China: Isotopic evidence from granulite xenoliths in Hannuoba, Sino-Korean craton. *Lithos* **62,** 111–124.

Zou H. B., Zindler A., Xu X. S., and Qi Q. (2000) Major, trace element, and Nd, Sr and. Pb isotope studies of Cenozoic basalts in SE China: Mantle sources, regional variations and tectonic significance. *Chem. Geol.* **171,** 33–47.